NATIONAL ADVISORY COMMITTEE FOR AERONAUTICS

REPORT No. 639

THE EFFECT OF COMPRESSIBILITY ON EIGHT FULL-SCALE PROPELLERS OPERATING IN THE TAKE-OFF AND CLIMBING RANGE

By DAVID BIERMANN and EDWIN P. HARTMAN

1938

AERONAUTIC SYMBOLS

1. FUNDAMENTAL AND DERIVED UNITS

	Symbol	Metric		English	
		Unit	Abbreviation	Unit	Abbreviation
Length_____	l	meter_____	m	foot (or mile)_____	ft. (or mi.)
Time_____	t	second_____	s	second (or hour)_____	sec. (or hr.)
Force_____	F	weight of 1 kilogram_____	kg	weight of 1 pound_____	lb.
Power_____	P	horsepower (metric)_____	_____	horsepower_____	hp.
Speed_____	V	{kilometers per hour_____	k.p.h.	miles per hour_____	m.p.h.
		{meters per second_____	m.p.s.	feet per second_____	f.p.s.

2. GENERAL SYMBOLS

W, Weight$=mg$

g, Standard acceleration of gravity$=9.80665$ m/s² or 32.1740 ft./sec.²

m, Mass$=\dfrac{W}{g}$

I, Moment of inertia$=mk^2$. (Indicate axis of radius of gyration k by proper subscript.)

μ, Coefficient of viscosity

ν, Kinematic viscosity

ρ, Density (mass per unit volume)

Standard density of dry air, 0.12497 kg-m⁻⁴-s² at 15° C. and 760 mm; or 0.002378 lb.-ft.⁻⁴ sec.²

Specific weight of "standard" air, 1.2255 kg/m³ or 0.07651 lb./cu. ft.

3. AERODYNAMIC SYMBOLS

S, Area

S_w, Area of wing

G, Gap

b, Span

c, Chord

$\dfrac{b^2}{S}$, Aspect ratio

V, True air speed

q, Dynamic pressure$=\dfrac{1}{2}\rho V^2$

L, Lift, absolute coefficient $C_L=\dfrac{L}{qS}$

D, Drag, absolute coefficient $C_D=\dfrac{D}{qS}$

D_0, Profile drag, absolute coefficient $C_{D_0}=\dfrac{D_0}{qS}$

D_i, Induced drag, absolute coefficient $C_{D_i}=\dfrac{D_i}{qS}$

D_p, Parasite drag, absolute coefficient $C_{D_p}=\dfrac{D_p}{qS}$

C, Cross-wind force, absolute coefficient $C_C=\dfrac{C}{qS}$

R, Resultant force

i_w, Angle of setting of wings (relative to thrust line)

i_t, Angle of stabilizer setting (relative to thrust line)

Q, Resultant moment

Ω, Resultant angular velocity

$\rho\dfrac{Vl}{\mu}$, Reynolds Number, where l is a linear dimension (e.g., for a model airfoil 3 in. chord, 100 m.p.h. normal pressure at 15° C., the corresponding number is 234,000; or for a model of 10 cm chord, 40 m.p.s., the corresponding number is 274,000)

C_p, Center-of-pressure coefficient (ratio of distance of c.p. from leading edge to chord length)

α, Angle of attack

ϵ, Angle of downwash

α_0, Angle of attack, infinite aspect ratio

α_i, Angle of attack, induced

α_a, Angle of attack, absolute (measured from zero-lift position)

γ, Flight-path angle

REPORT No. 639

THE EFFECT OF COMPRESSIBILITY ON EIGHT FULL-SCALE PROPELLERS OPERATING IN THE TAKE-OFF AND CLIMBING RANGE

By DAVID BIERMANN and EDWIN P. HARTMAN

Langley Memorial Aeronautical Laboratory

NATIONAL ADVISORY COMMITTEE FOR AERONAUTICS

HEADQUARTERS, NAVY BUILDING, WASHINGTON, D. C.

LABORATORIES, LANGLEY FIELD, VA.

Created by act of Congress approved March 3, 1915, for the supervision and direction of the scientific study of the problems of flight (U. S. Code, Title 50, Sec. 151). Its membership was increased to 15 by act approved March 2, 1929. The members are appointed by the President, and serve as such without compensation.

JOSEPH S. AMES, Ph. D., *Chairman*,
Baltimore, Md.

DAVID W. TAYLOR, D. Eng., *Vice Chairman*,
Washington, D. C.

WILLIS RAY GREGG, Sc. D., *Chairman, Executive Committee*,
Chief, United States Weather Bureau.

WILLIAM P. MacCRACKEN, J. D., *Vice Chairman, Executive Committee*,
Washington, D. C.

CHARLES G. ABBOT, Sc. D.,
Secretary, Smithsonian Institution.

LYMAN J. BRIGGS, Ph. D.,
Director, National Bureau of Standards.

ARTHUR B. COOK, Rear Admiral, United States Navy,
Chief, Bureau of Aeronautics, Navy Department.

HARRY F. GUGGENHEIM, M. A.,
Port Washington, Long Island, N. Y.

SYDNEY M. KRAUS, Captain, United States Navy,
Bureau of Aeronautics, Navy Department.

CHARLES A. LINDBERGH, LL. D.,
New York City.

DENIS MULLIGAN, J. S. D.,
Director of Air Commerce, Department of Commerce.

AUGUSTINE W. ROBINS, Brigadier General, United States Army,
Chief Matériel Division, Air Corps, Wright Field, Dayton, Ohio.

EDWARD P. WARNER, Sc. D.,
Greenwich, Conn.

OSCAR WESTOVER, Major General, United States Army,
Chief of Air Corps, War Department.

ORVILLE WRIGHT, Sc. D.,
Dayton, Ohio.

GEORGE W. LEWIS, *Director of Aeronautical Research*

JOHN F. VICTORY, *Secretary*

HENRY J. E. REID, *Engineer-in-Charge, Langley Memorial Aeronautical Laboratory, Langley Field, Va.*

JOHN J. IDE, *Technical Assistant in Europe, Paris, France*

TECHNICAL COMMITTEES

AERODYNAMICS

POWER PLANTS FOR AIRCRAFT

AIRCRAFT MATERIALS

AIRCRAFT STRUCTURES

AIRCRAFT ACCIDENTS

INVENTIONS AND DESIGNS

Coordination of Research Needs of Military and Civil Aviation

Preparation of Research Programs

Allocation of Problems

Prevention of Duplication

Consideration of Inventions

LANGLEY MEMORIAL AERONAUTICAL LABORATORY

LANGLEY FIELD, VA.

Unified conduct, for all agencies, of scientific research on the fundamental problems of flight.

OFFICE OF AERONAUTICAL INTELLIGENCE

WASHINGTON, D. C.

Collection, classification, compilation, and dissemination of scientific and technical information on aeronautics.

REPORT No. 639

THE EFFECT OF COMPRESSIBILITY ON EIGHT FULL-SCALE PROPELLERS OPERATING IN THE TAKE-OFF AND CLIMBING RANGE

By David Biermann and Edwin P. Hartman

SUMMARY

Tests were made of eight full-scale propellers of different shape at various tip speeds up to about 1,000 feet per second. The range of blade-angle settings investigated was from 10° to 30° at the 0.75 radius.

The results indicate that a loss in propulsive efficiency occurred at tip speeds from 0.5 to 0.7 the velocity of sound for the take-off and climbing conditions. As the tip speed increased beyond these critical values, the loss rapidly increased and amounted, in some instances, to more than 20 percent of the thrust power for tip-speed values of 0.8 the speed of sound. In general, as the blade-angle setting was increased, the loss started to occur at lower tip speeds. The maximum loss for a given tip speed occurred at a blade-angle setting of about 20° for the take-off and 25° for the climbing condition.

Although the loss at the take-off condition due to compressibility was greater for the R. A. F. 6 section than for the Clark Y, greater for blades of standard width than for extremely wide ones, and greater for a thick propeller than for a thin one, the actual efficiencies at high tip speeds were found to be about the same because, in each case, the propeller that had the greatest losses from increasing the tip speed had the highest efficiency at low tip speeds.

The compressibility loss at the take-off for controllable propellers was considerably reduced because of decreased blade-angle operation necessitated by increased power coefficients, but the reverse was true for fixed-pitch propellers inasmuch as the higher power coefficients resulted in reduced engine speeds.

A simplified method for correcting propellers for the effect of compressibility is given in an appendix.

INTRODUCTION

The first effects of the compressibility of air to influence the flight of airplanes are felt by the tips of propeller blades, which usually operate at speeds approaching that of sound. The results of experience and research agree in showing that at sonic tip speeds the effects of compressibility are very unfavorable. The flying speeds of airplanes have only recently reached values where the effects of compressibility on parts of the airplane other than the propeller are of such magnitude as to warrant more than passing attention. The serious effects of high tip speeds on the performance of propellers have, however, been of great practical inter-est for many years and considerable research has been directed toward a better understanding of the phenomena of compressibility as affecting propeller operation. The principal methods of attacking the problem may be classified as: (a) airfoil tests, (b) model-propeller tests, and (c) full-scale-propeller tests.

Airfoil tests are particularly valuable in the study of compressibility because many of the variables present in propeller tests do not enter into airfoil tests and the important compressibility effects are therefore more easily isolated and revealed. Without them the compressibility phenomena detected in propeller tests would be difficult to understand or to explain.

An examination of references 1, 2, and 3 reveals a marked change in airfoil characteristics with increasing air speed. There appears to be a general tendency for the slope of the lift curves and of the profile drag in the usual propeller operating range to increase up to some critical value of V/V_c (ratio of air speed to the speed of sound) corresponding to that at which the compressibility burble occurs and at which the lift drops sharply and the drag increases rapidly. The value of the speed at which the compressibility burble occurs is dependent on the angle of attack and the thickness of the airfoil; increasing either of these quantities causes the compressibility burble to occur at lower speeds, sometimes as low as 0.4 or 0.5 the speed of sound. The compressibility burble is attributed to the formation of a shock wave caused when the flow over the surface exceeds the local velocity of sound. (See reference 4.) A large part of the kinetic energy in the flow is converted into heat when the particles of air pass through the shock region, which results in an increased drag of the airfoil. Also, the reduction in velocity and the consequent increase in pressure behind the shock wave result in reduced lift.

The influence of compressibility on the characteristics of model propellers has been observed in many British tests (reference 5). The results of propeller tests agreed qualitatively with the results of airfoil tests in that the power and the thrust increased with tip speed up to a critical value beyond which the thrust and the efficiency dropped.

There is some reason to believe that the propeller characteristics should depend on Reynolds Number as well as on tip speed; however, tests of propellers of

1

different blade width (reference 6) show only a slight Reynolds Number effect, and British flight tests, which were made to check model tests (reference 7), indicate no serious scale effect at the peak-efficiency condition.
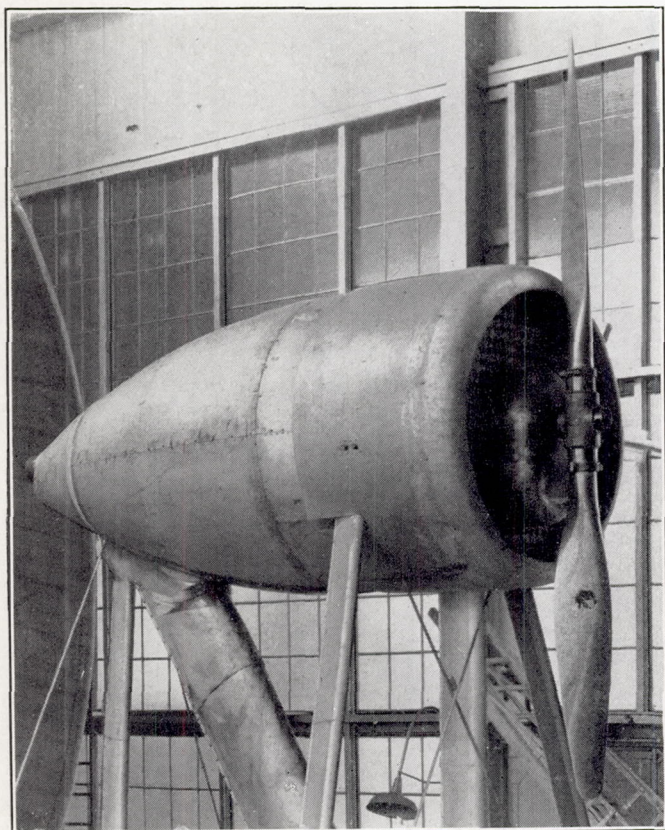
Four of the propellers tested have Clark Y blade sections and four have R. A. F. 6 sections. Of the Clark Y propellers, three are of a series having variations in thickness ratio. Among the R. A. F. 6 propellers there are variations in blade width and plan form.
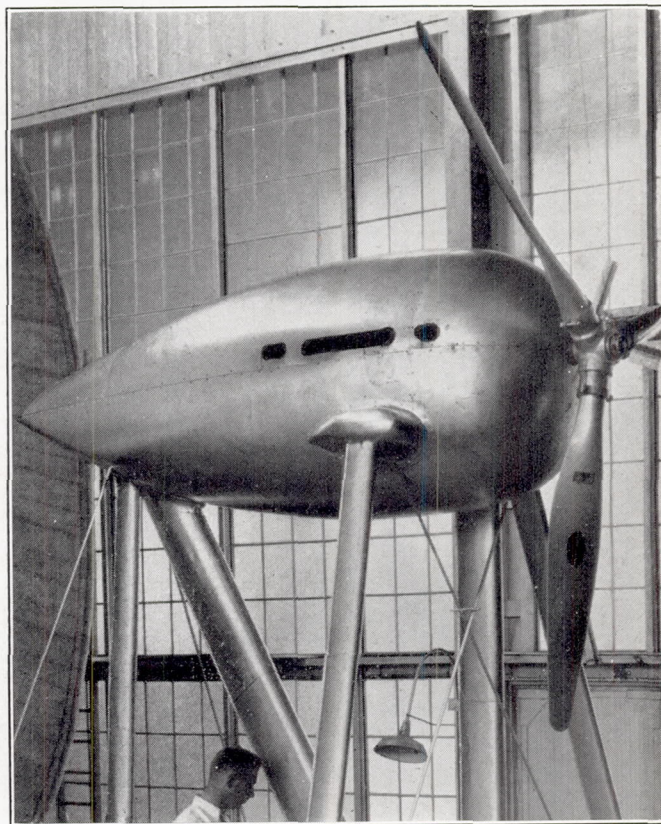

FIGURE 1.—The propeller test set-up with radial-engine nacelle.

FIGURE 2.—The test set-up showing liquid-cooled engine nacelle.

Wind-tunnel tests have been made by the N. A. C. A. of a series of full-scale propellers having different thickness ratios and different airfoil sections (reference 8). For the low blade-angle settings investigated (6.8°, 9.6°, and 10°) there was discovered little or no loss in efficiency below a tip speed of about 1,000 feet per second, even in the low V/nD range. In view of the results from later tests of the same airfoil sections (reference 2), it would appear that compressibility effects of appreciable magnitude should be noticed for higher blade angles in the low V/nD range corresponding to the take-off and climbing conditions of flight.

The tests reported herein were instituted to determine the compressibility effect on full-scale propellers operating at blade angles corresponding to those used in present-day aircraft when set for the take-off and climbing conditions. The blade-angle settings investigated ranged from 10° to 30° in 5° increments. Owing to the limiting tunnel speed of about 115 miles per hour, the upper V/nD range could not be obtained for the higher tip-speed runs; however, the V/nD range corresponding to the take-off and climbing conditions of flight was covered. The tip-speed range extended from about 600 feet per second to more than 1,000 feet per second for one propeller.

These compressibility tests were run from time to time as a part of a propeller program involving a number of subjects. During this period of time, the body that covered the engine was changed from a radial engine nacelle to a liquid-cooled engine nacelle. Several of the propellers were tested in conjunction with the radial engine nacelle and some with the liquid-cooled engine nacelle; a few propellers were tested in conjunction with both.

The series of tests reported herein, although not complete nor entirely conclusive, covers a very important field. Research on the problem of compressibility should be continued to investigate further such effects as may be caused by changes in blade section, thickness, and width and should be extended to higher values of tip speed, especially for the upper ranges of blade angles.

APPARATUS AND METHODS

The tests were made in the propeller-research tunnel, a description of which is given in reference 9. The power to operate the test propellers was supplied by a 600-horsepower Curtiss Conqueror engine geared 7:5.

The engine was boosted to 800 horsepower, when more power was required, by a motor-driven Roots blower located on the floor of the test chamber.

The dynamometer used for measuring torque is of the cradle type with the axis of rotation on one side of the engine. The torque reaction was carried through a vertical compression post to a mechanical balance on the floor of the test chamber. The engine cowling was supported on the fixed portion of the supporting frame.

The radial engine cowling (fig. 1) used for the first series of tests is 52 inches in maximum diameter and 126 inches in length. The liquid-cooled engine nacelle (fig. 2) is oval in cross section, 43 inches in height, 38 inches in width, and 126 inches in length.

Eight propellers having a range of diameters from $9\frac{1}{2}$ feet to 11 feet were tested. The distinguishing features of these propellers are shown in figure 3. Blade-form curves are given in figures 4, 5, and 6. The symbols used in these figures are defined as:

D, diameter.
R, radius to the tip.
r, station radius.
b, section chord.
h, section thickness.
p, geometric pitch.

All the propellers have two blades. Section ordinates are given in figure 7. The principal dimensions of the propellers are given in the following table.

Propeller	Diameter (ft.)-(in.)	Section	$\frac{b}{D}$ at 0.75 R	$\frac{h}{b}$ at 0.75 R	Tip shape
5868–9	10–0	Clark Y (new)	0.061	0.090	Round.
5868–R6	10–0	R. A. F. 6	.061	.090	Do.
4877	9–6	Clark Y (old)	.053	.06	Do.
4878	9–6	do	.053	.08	Do.
4879	9–6	do	.053	.10	Do.
4371	11–0	R. A. F 6	.053	.080	Do.
195	11–0	do	.050	.067	Pointed.
37–3647	10–0	do	.092	.090	Round.
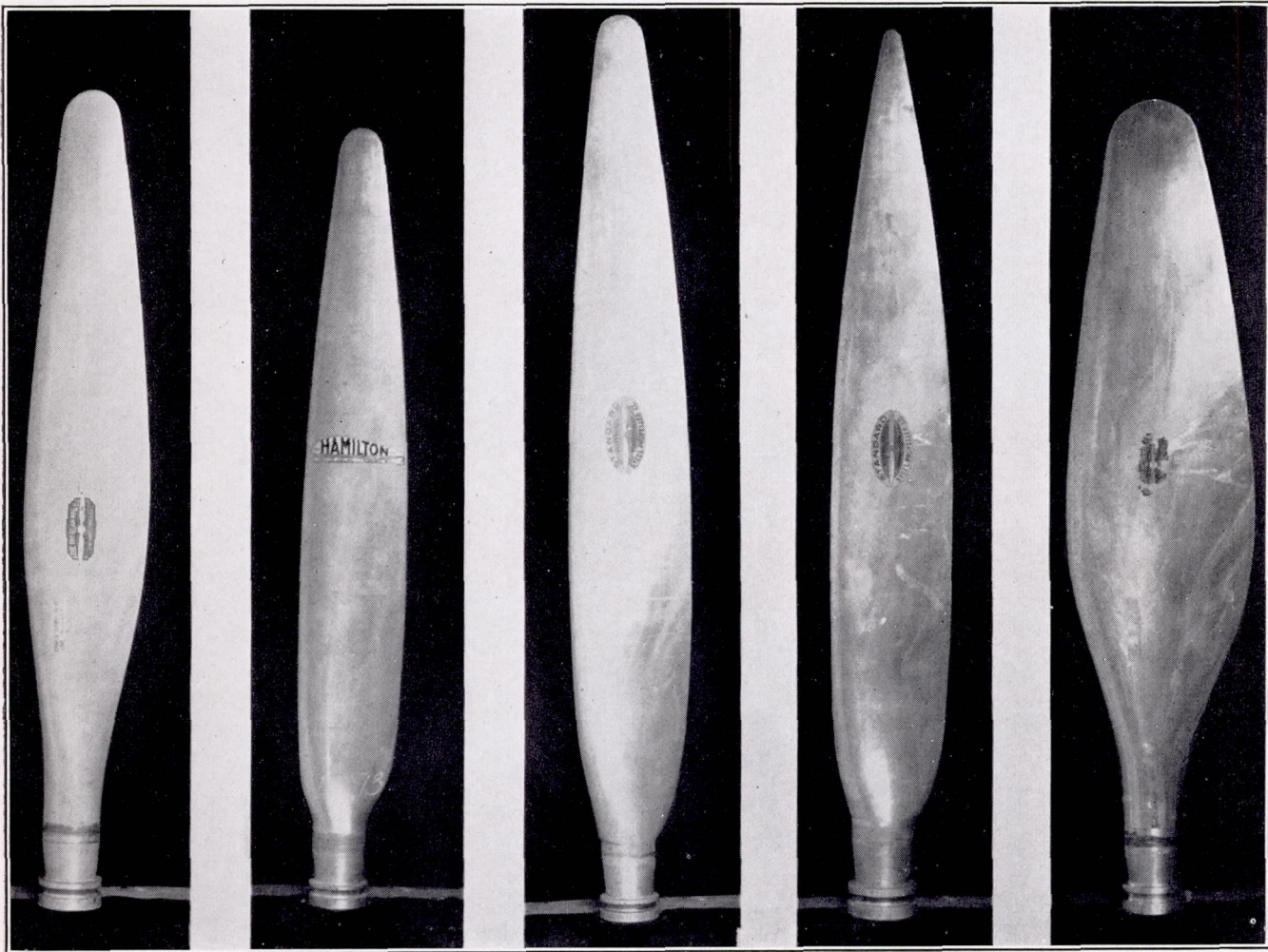
5868–9
5868–R6

4877
4878
4879

4371

195

37–3647

FIGURE 3.—Propeller blades tested.

The method adopted in making these tests consisted in setting the engine speed at a given value and increasing the tunnel air speed progressively up to the propeller minus the body and interference drag, and tunnel air speed. The drag of the body was measured in a separate test with the propeller removed.
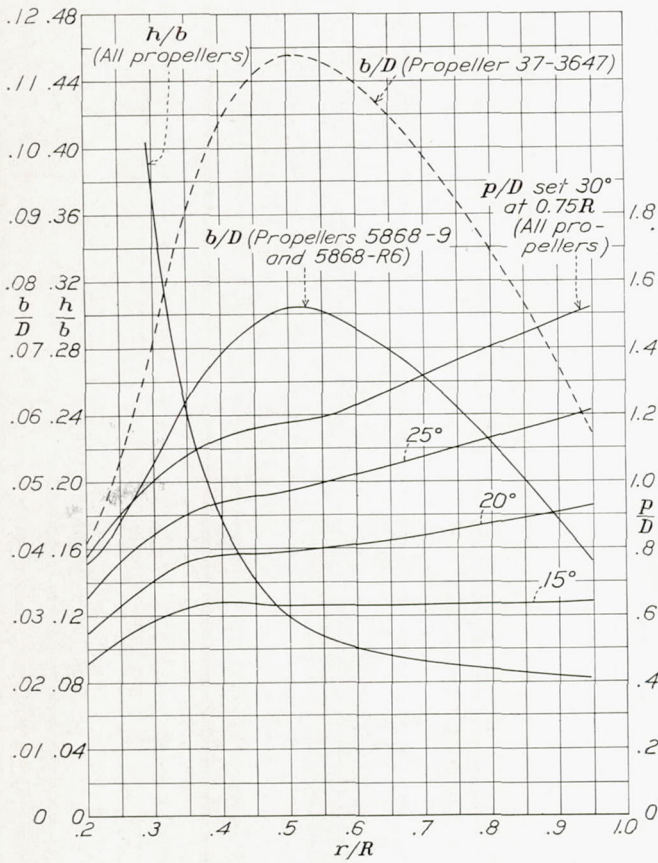

FIGURE 4.—Blade-form curves for propellers 5868–R6, 5868–9, and 37–3647.
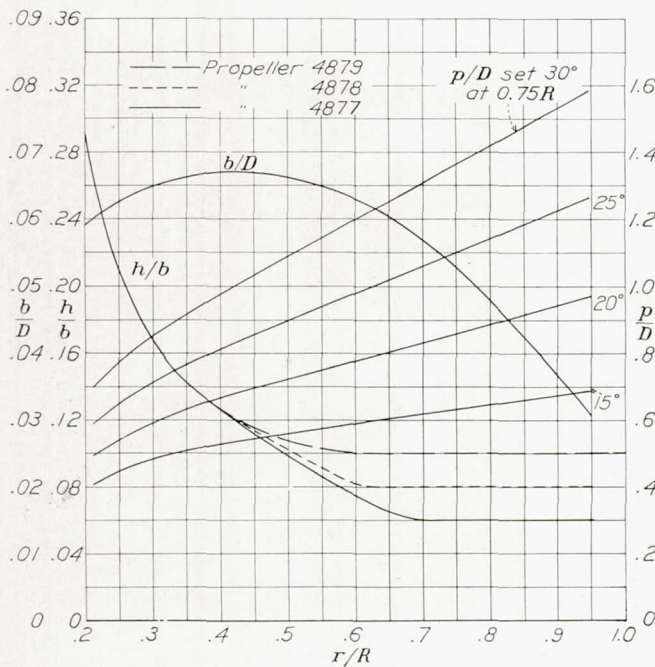

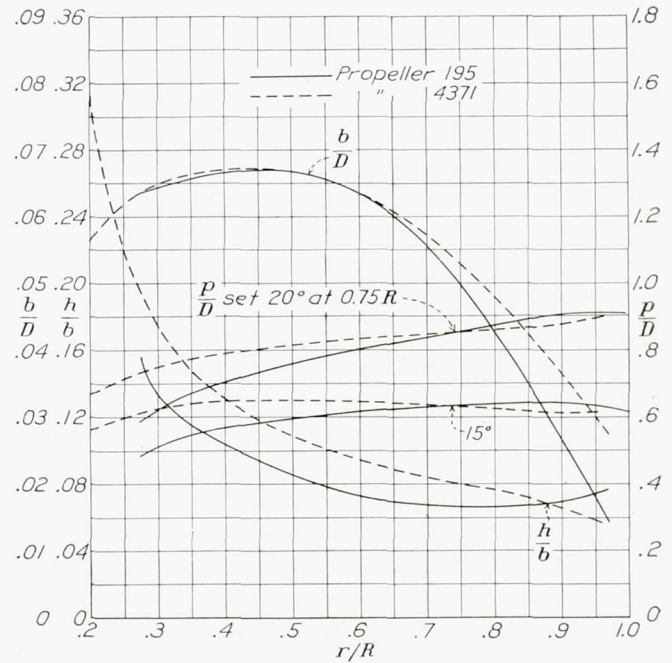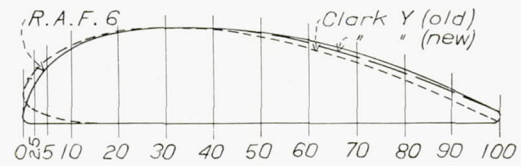FIGURE 5.—Blade-form curves for propellers 4877, 4878, and 4879.

FIGURE 6.—Blade-form curves for propellers 195 and 4371.

Station	R. A. F. 6, Upper	Clark Y (old)		Clark Y (new)	
		Upper	Lower	Upper	Lower
2.5	0.41	0.56	0.13	0.55	0.13
5	.59	.68	.08	.67	.08
10	.79	.82	.04	.81	.04
20	.95	.97	0	.96	.01
30	1.00	1.00	0	1.00	0
40	.99	.98	0	.99	0
50	.95	.90	0	.93	0
60	.87	.78	0	.83	0
70	.74	.63	0	.69	0
80	.56	.45	0	.52	0
90	.35	.24	0	.34	0
L. E. radius	.10	0.13		0.15	
T. E. radius	.077	.005	0	.077	0

FIGURE 7.—Propeller section ordinates (in fraction of maximum ordinate).

RESULTS

The measured values have been reduced to the usual coefficients of thrust, power, and propulsive efficiency,

$$C_T = \frac{\text{effective thrust}}{\rho n^2 D^4}$$

$$C_P = \frac{\text{engine power}}{\rho n^3 D^5}$$

and

$$\eta = \frac{C_T}{C_P} \frac{V}{nD}$$

where the effective thrust is the measured thrust plus the body drag with no propeller or, in other words, the propeller shaft tension minus the increment of body drag due to the slipstream.

maximum value of about 115 miles per hour. The principal measurements recorded include: engine torque, propeller rotational speed, thrust of the

D, propeller diameter, ft.

n, propeller rotational speed, r. p. s.

The foregoing coefficients were plotted against the coefficient V/nD and a smooth curve was drawn through the thrust and power points. The efficiency curve was adjusted to correspond to the thrust and power curves as well as to the calculated efficiency points. A typical plot is shown in figure 8.
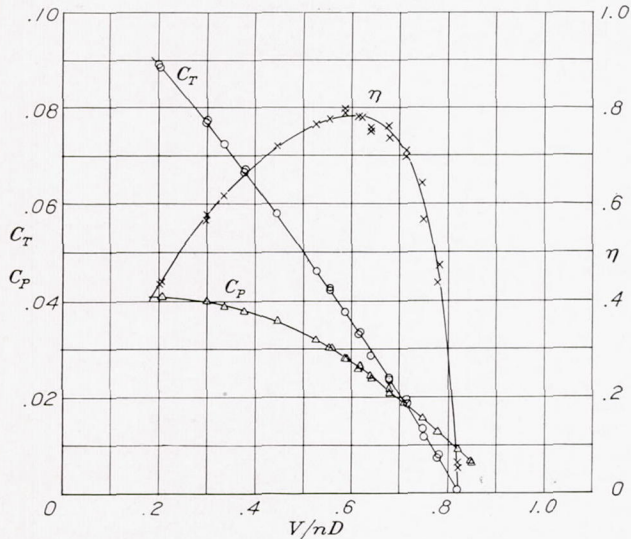

FIGURE 8.—Typical test results showing normal scatter of points. Propeller 5868–R6; diameter, 10 ft.; propeller set 15° at 0.75R; propeller speed, 1,200 r. p. m.; liquid-cooled engine nacelle.

In order to show the effect of different tip speeds on the propeller characteristics for particular values of V/nD, plots are given of relative efficiency, relative thrust, and relative power against the ratio of the tip speed to the speed of sound, V'/V_c. Only two types of such plots are given: one represents the take-off condition of a landplane arbitrarily taken at a V/nD value of 0.30 times the V/nD for peak efficiency; and the other, the climbing condition taken at a V/nD value of 0.65 times the V/nD for peak efficiency. The reference point used in computing the relative values of efficiency, thrust, and power was $V'/V_c=0.5$. Thus

$$\frac{\eta}{\eta_{\left(\frac{V'}{V_c}=0.5\right)}}, \frac{C_T}{C_{T\left(\frac{V'}{V_c}=0.5\right)}}, \text{ and } \frac{C_P}{C_{P\left(\frac{V'}{V_c}=0.5\right)}} \text{ represent the ratios}$$

of the propeller characteristics with respect to those at a tip-speed ratio of $V'/V_c=0.5$. The tip-speed velocity V' is the tangential component of the actual tip speed and is defined by the relation $V'=\pi nD$. The forward component of the tip speed, which increases with V/nD, was small enough to be neglected in the present tests.

The test results are given in three groups: The first group (figs. 9 to 35) covers the work done with the radial-engine cowled nacelle. The second group (figs. 36 to 46) covers the results with the liquid-cooled engine nacelle. The third group (figs. 47 to 53) comprises comparisons and examples derived from the first two groups. The test results have been tabulated in six tables and are available on request from the National Advisory Committee for Aeronautics.

Inasmuch as the temperature of the air determines the velocity of sound, the following table of temperatures is included.

Liquid-cooled engine nacelle			Radial engine nacelle						
			Unsupercharged (including all propeller speeds, except those noted under "Supercharged")			Supercharged			
Propeller	Blade angle (deg.)	Temperature (°F.)	Propeller	Blade angle (deg.)	Temperature (°F.)	Propeller	Blade angle (deg.)	Propeller speed (r. p. m.)	Temperature (°F.)
5868–R6 {	15	88	5868–9 {	15	66	5868–9 {	20	1,725	65
	20	89		20	65		25	1,500	71
37–3647 {	15	93		25	64		25	1,600	71
	20	97		30	64		30	1,300	70
4877	20	88	5868–R6 {	15	53	5868–R6 {	15	1,800	81
4878	20	84		20	54		20	1,750	68
4879	20	84		25	61		25	1,555	69
				30	72		30	1,300	73
			4879 {	15	66	4371 {	15	1,700	77
				20	59		20	1,550	69
				25	61	195 {	15	1,800	75
				30	72		20	1,600	66
			4371 {	15	71				
				20	81				
			195 {	15	78				
				20	76				

The speed of sound in air is given by the following formulas:

$$V_c = 1{,}120\sqrt{T_C/288}$$
$$= 1{,}120\sqrt{T_F/518.4}$$

where

T_C is absolute temperature, °C.

T_F, absolute temperature, °F.

DISCUSSION

An examination of the results from airfoil tests at high speeds, such as are given in reference 2, leads to the following conclusions regarding what should be expected from propeller tests:

(a) The thrust and power coefficients should increase with tip speed in the range below the critical tip speed (compressibility burble).

(b) There should be a loss of thrust and efficiency and an increase in power after the tip speed exceeds the critical value.

(c) Since compressibility losses occur at lower speeds as the angle of attack of the airfoil is increased, it follows that, at low values of V/nD, losses should occur at fairly low tip speeds. The critical tip speed for a given blade angle should increase as V/nD is increased.
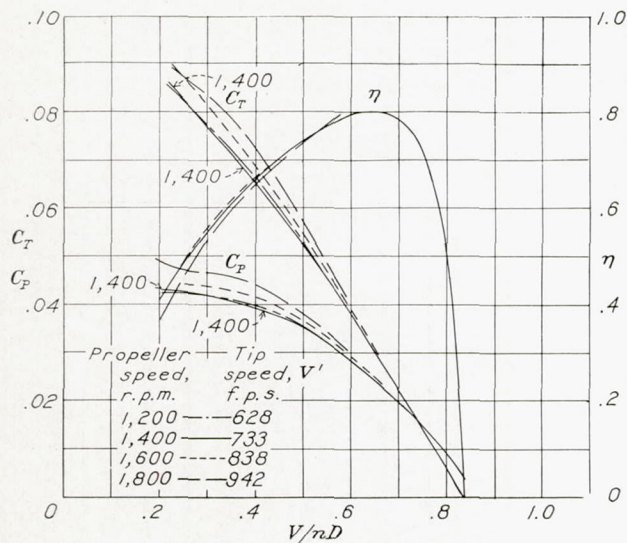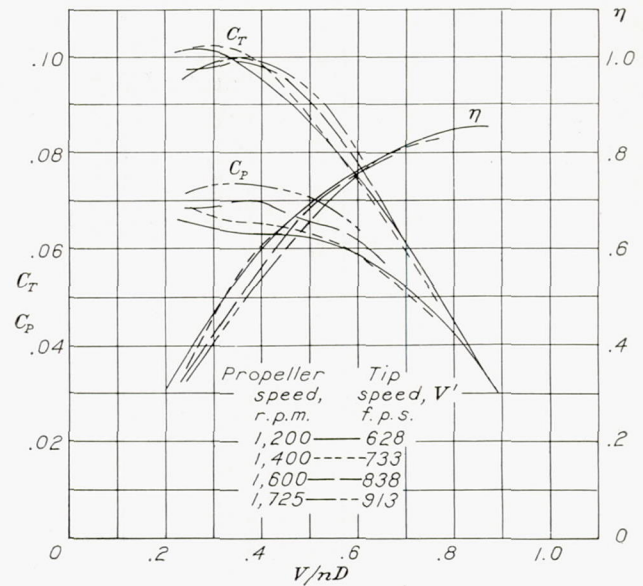
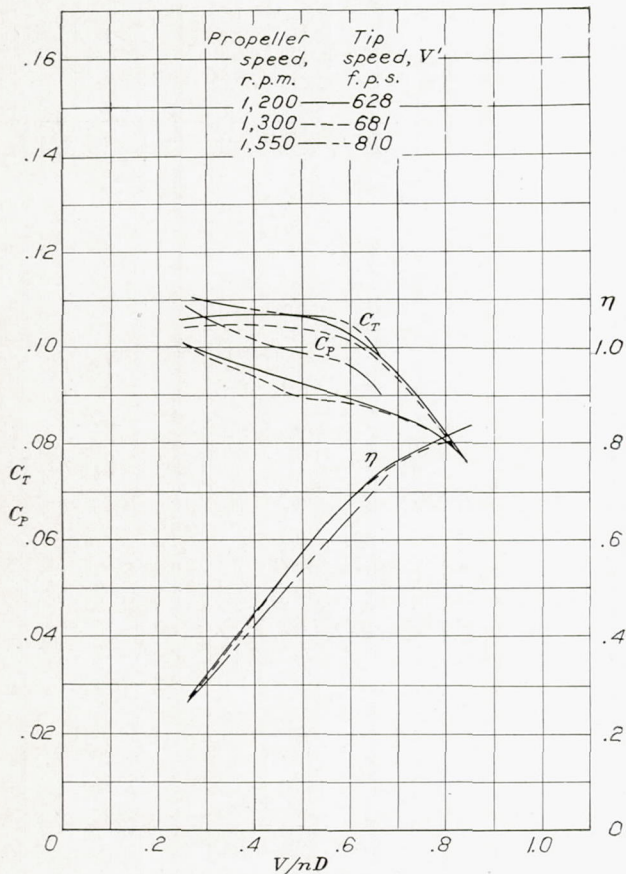FIGURE 9.—Propeller set 15° at 0.75R.

FIGURE 10.—Propeller set 20° at 0.75R.

FIGURE 11.—Propeller set 25° at 0.75R.
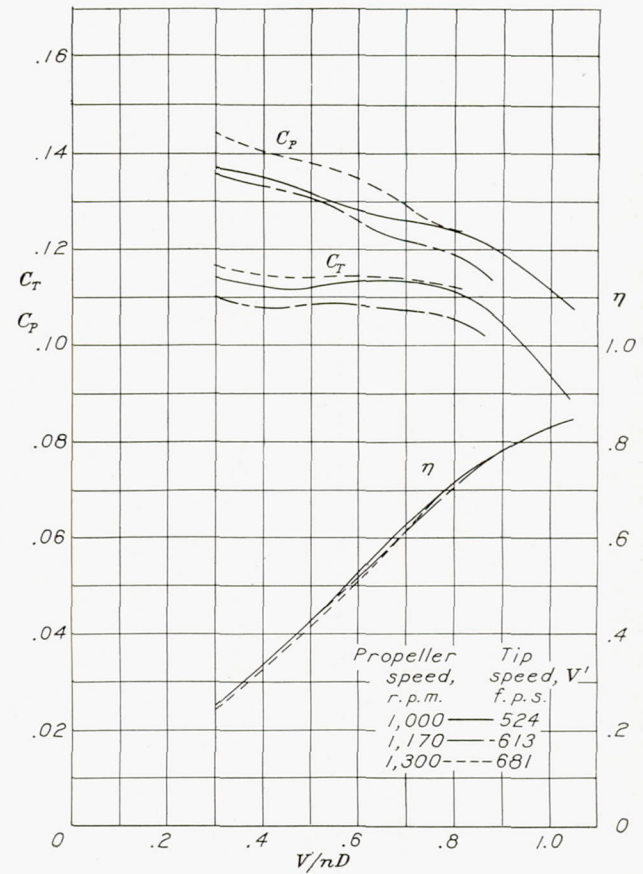
FIGURE 12.—Propeller set 30° at 0.75R.

FIGURES 9 to 12.—Effect of compressibility on propeller characteristics. Propeller 5868-9; diameter, 10 ft.; radial engine nacelle.

(d) The blade-angle setting of the propeller should determine the V/nD range wherein compressibility losses occur for any given tip speed, because the section angle of attack is determined by both the V/nD and the blade-angle setting. For blade angles sufficiently low that stalling never occurs (approximately 20° and less), the greatest loss should occur at a zero value of V/nD. For higher value of the blade angle, the normal stall might be expected to delay the compressibility burble so that losses from this source might, in general, be confined to the V/nD range below the stall. Under such conditions the climbing condition of flight might suffer
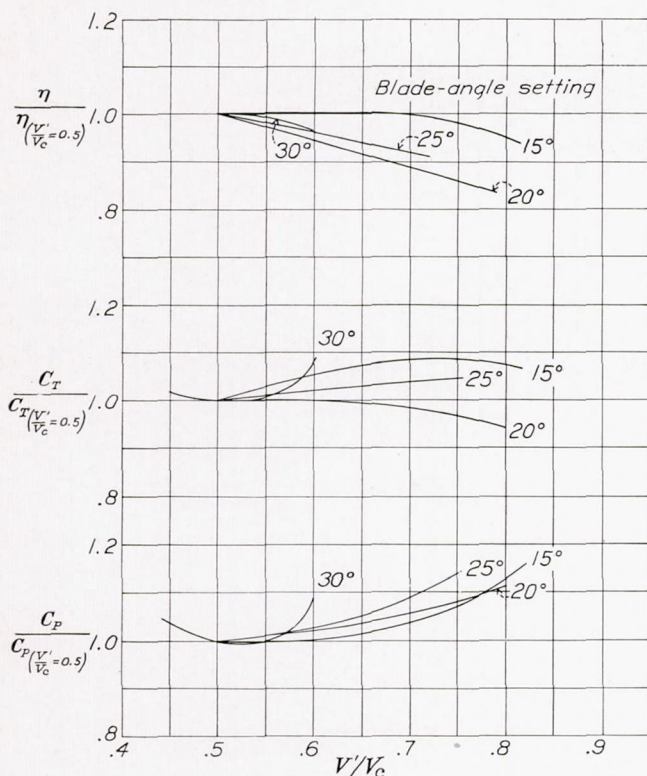

FIGURE 13.—Changes in propeller characteristics due to compressibility for the take-off condition. Propeller 5868–9; diameter, 10 ft.; radial engine nacelle; $\frac{V}{nD} = 0.30 \left(\frac{V}{nD} \right)_{peak\ eff.}$

more from compressibility than the take-off condition.

(e) The Clark Y section has a higher critical speed than the R. A. F. 6 section and propellers of Clark Y section should therefore be less affected by compressibility in the normal operating range; likewise, thin propellers should be less affected than thick ones.

A general survey of the results reveals qualitative agreement between airfoil and full-scale-propeller results. There might be some question as to whether the effects noted are entirely due to compressibility, since blade deflection would result in somewhat the same displacement of the curves. Some deflection measurements that were made by a light-beam method showed the blade torsional deflection to be negligible; it is therefore probable that the various effects noted are due to compressibility.

80780—39——2

EFFECTS AT SPEEDS BELOW THE CRITICAL

The tendency for the thrust and power coefficients, at a given V/nD to increase with increasing tip speed for speeds below the critical may be noted for nearly all of the propellers. The increase is greatest at low V/nD values and tends to diminish as V/nD is increased. This effect is of some importance in the take-off and climb of both fixed-pitch and controllable propellers. In the case of the fixed-pitch propeller, the engine speed will be reduced by the higher power requirements of the propeller and engine power will be
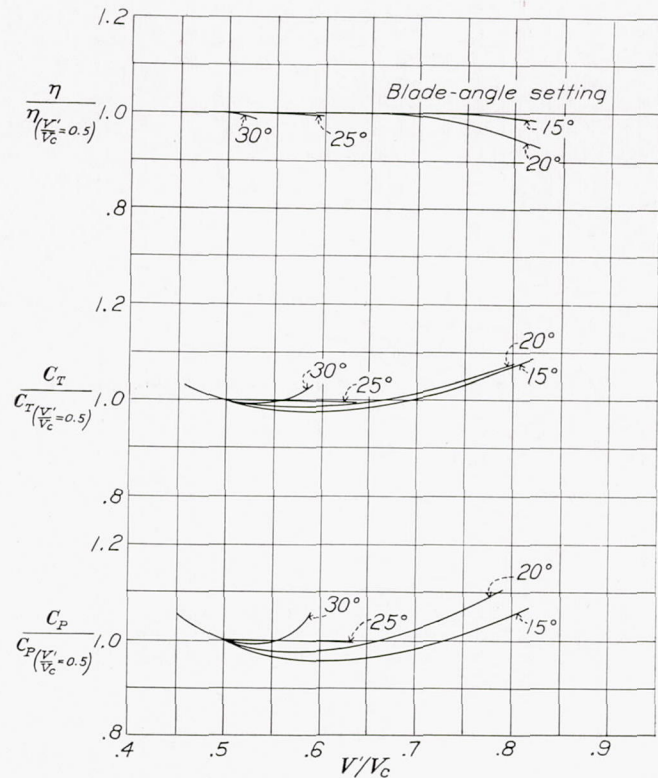

FIGURE 14.—Changes in propeller characteristics due to compressibility for the climbing condition. Propeller 5868–9; diameter, 10 ft.; radial engine nacelle; $\frac{V}{nD} = 0.65 \left(\frac{V}{nD} \right)_{peak\ eff.}$

lost proportionately to the drop in rotational speed. The pitch of the controllable propeller must be reduced to offset the added power required with the result that the propulsive efficiency will be increased.

EFFECT AT SPEEDS ABOVE THE CRITICAL

At the tip speeds at which compressibility losses occur at the tips, the tendency for the thrust coefficient to continue to increase is reduced. After sufficient blade area at the tips is operating beyond the compressibility stall, there is a tendency for the thrust coefficient to decrease with increasing tip speed and for the power coefficient to rise disproportionately fast. A consistent reduction in efficiency may be noted for all the propellers after the tip speed has reached some critical value. The amount of reduction can be seen to depend upon a number of factors, such as tip speed, V/nD range,
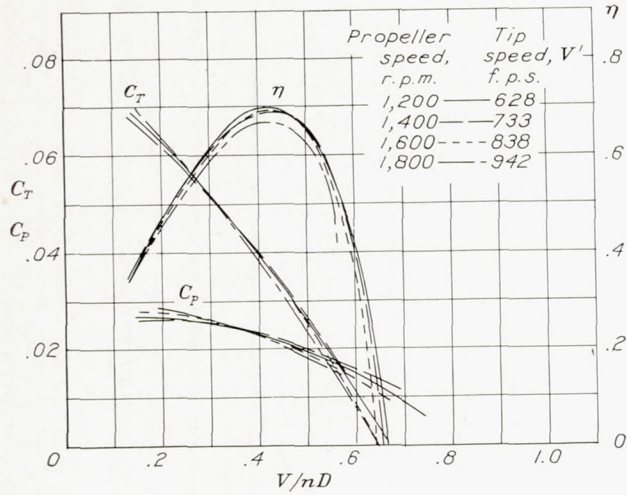
FIGURE 15.—Propeller set 10° at 0.75R.

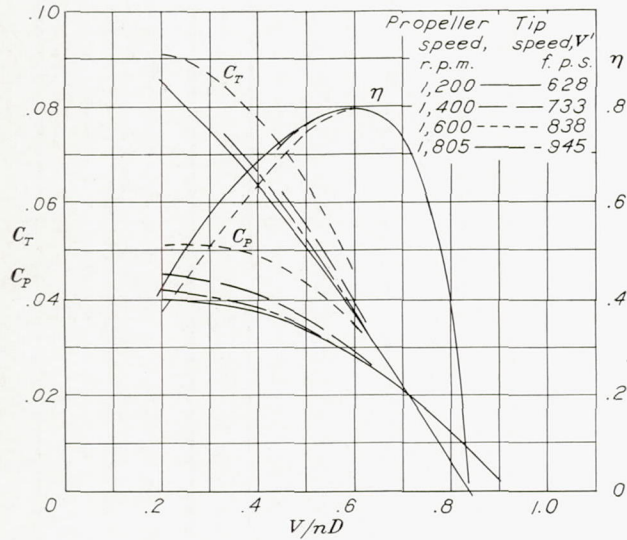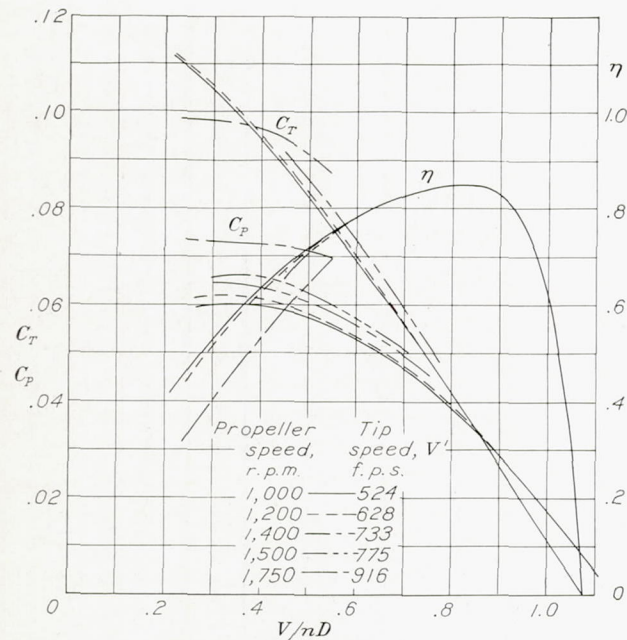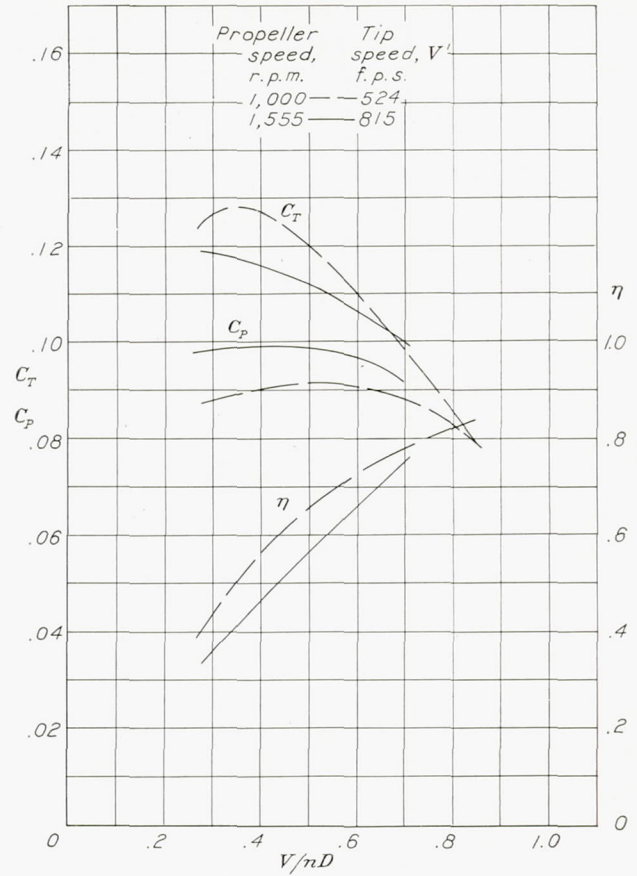FIGURE 16.—Propeller set 15° at 0.75R.

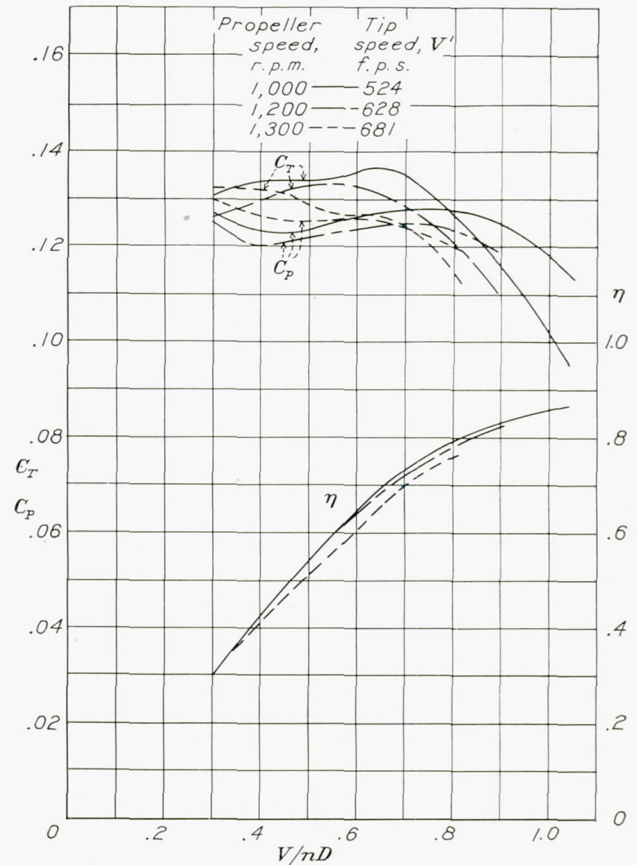FIGURE 17.—Propeller set 20° at 0.75R.

FIGURE 18.—Propeller set 25° at 0.75R.

FIGURE 19.—Propeller set 30° at 0.75R.

FIGURES 15 to 19.—Effect of compressibility on propeller characteristics. Propeller 5868–R6; diameter, 10 ft.; radial engine nacelle.

blade-angle setting, blade section, blade width, and blade thickness.

Tip speed.—The tip speed at which compressibility losses first appear varies quite widely, depending principally on the V/nD range and the blade-angle setting, which, of course, defines the angle of attack of the sections. In the take-off range of V/nD, it may be noted that compressibility losses first become evident at from 0.5 to 0.7 the speed of sound for the different propellers. (See figs. 13, 20, 26, 30, etc.) The blade-angle setting evidently has little effect in this range as no definite trends are evident except, perhaps, in the case of propeller 5868–R6 (fig. 20), which shows the results for a wider range of blade-angle settings than the other propellers.
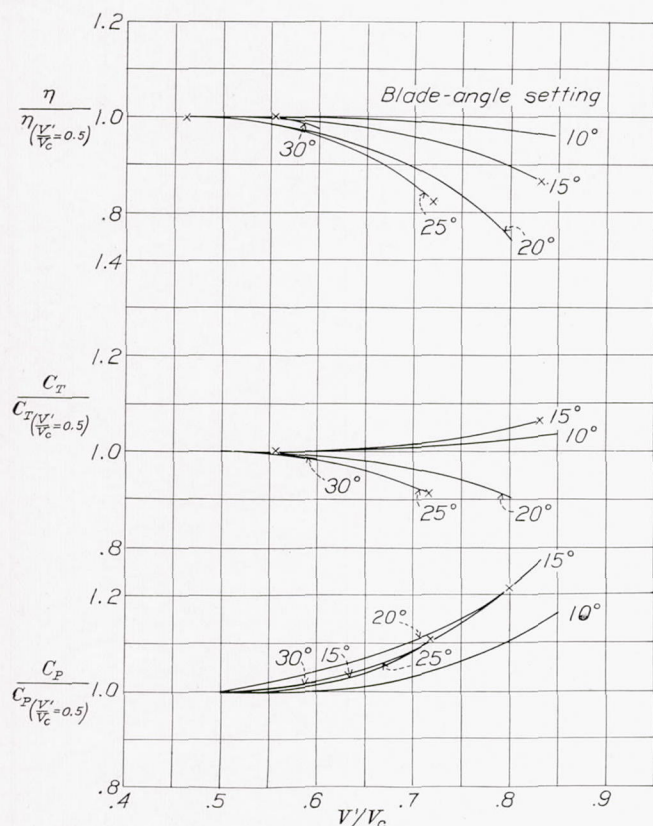

FIGURE 20.—Changes in propeller characteristics due to compressibility for the take-off condition. Propeller 5868–R6; diameter, 10 ft.; radial engine nacelle; $\frac{V}{nD}=0.30\left(\frac{V}{nD}\right)_{peak\ eff.}$

In the climbing range of V/nD, compressibility losses first appear at tip-speed values of from 0.6 to 0.75 the speed of sound for most propellers. (See figs. 14, 21, 27, 31, etc.) In general, as the pitch is increased, the losses occur at lower tip speeds. (See, in particular, figs. 14 and 27.)

Blade-angle setting.—The magnitude of the compressibility loss is largely determined by the blade-angle setting for any given tip speed and V/nD range. In the take-off range, the indications are that the greatest loss occurs at blade-angle settings of about 20°. (See

figs. 13, 20, and 26.) At tip speeds of $0.8V_c$, the maximum indicated losses amount to from 10 to 25 percent of the thrust power, depending upon the propeller. Extrapolation of some of the curves to tip speeds of $0.9V_c$ indicates that the maximum loss might amount to as much as 40 percent.

In the climbing range, the greatest loss evidently occurs at a blade-angle setting of about 25°. Since the engine power was limited, it was not possible to reach very high tip speeds for these settings. The 9½-foot propeller (4879) afforded the best opportunity to study the effects. A tip speed of nearly $0.8V_c$ was reached for the 25° setting and, from this test (fig. 27), the foregoing statement is best substantiated. The maximum loss in efficiency for this condition appears to be of the order of 10 percent at tip speeds of $0.8V_c$.
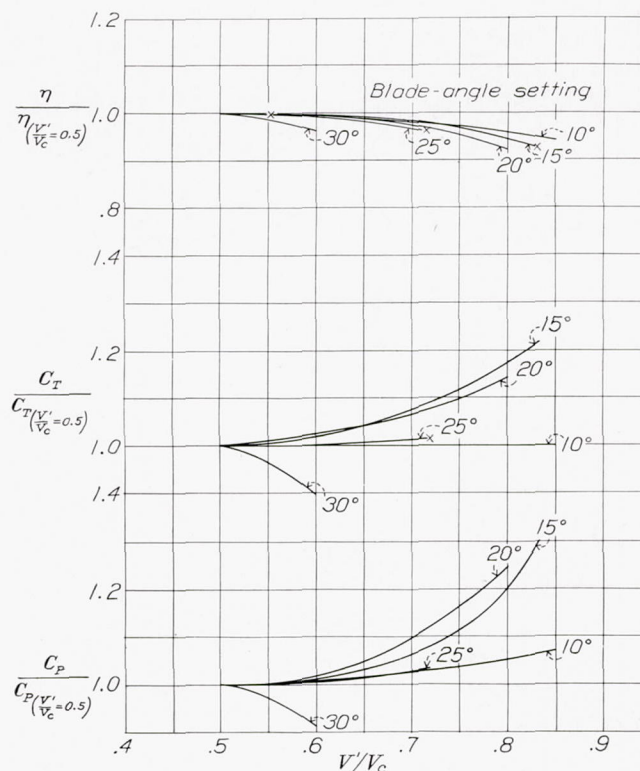

FIGURE 21.—Changes in propeller characteristics due to compressibility for the climbing condition. Propeller 5868–R6; diameter, 10 ft.; radial engine nacelle; $\frac{V}{nD}=0.65\left(\frac{V}{nD}\right)_{peak\ eff.}$

Blade section.—Of the eight propellers tested, four have Clark Y sections and four have R. A. F. 6 sections. Only two of these can be directly compared for the effect of section, however, because the rest also differ in other respects. In figure 47 a comparison is made between the two propellers 5868–9 and 5868–R6 on the basis of the relative take-off and climbing efficiencies. It may be noted that, for any given tip speed, the losses for the Clark Y propeller are, in general, only about one-third to one-half as much as for the R. A. F. 6 propeller. The actual efficiencies in the take-off and climbing ranges are, however, about equal
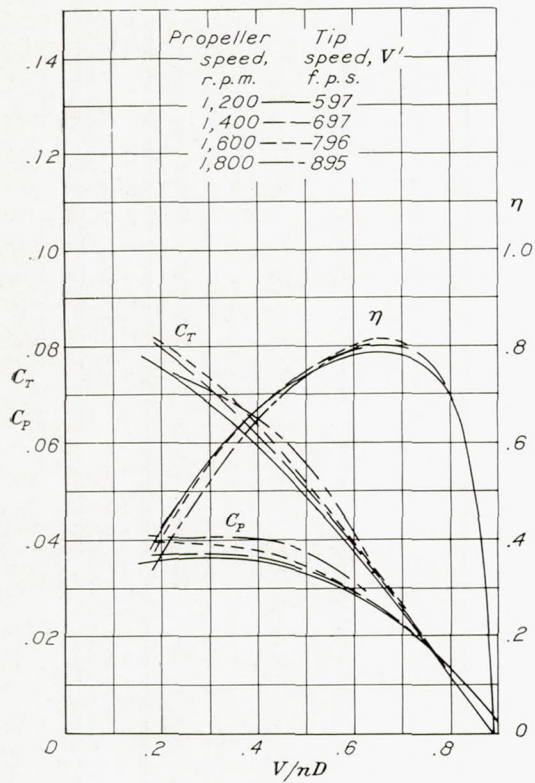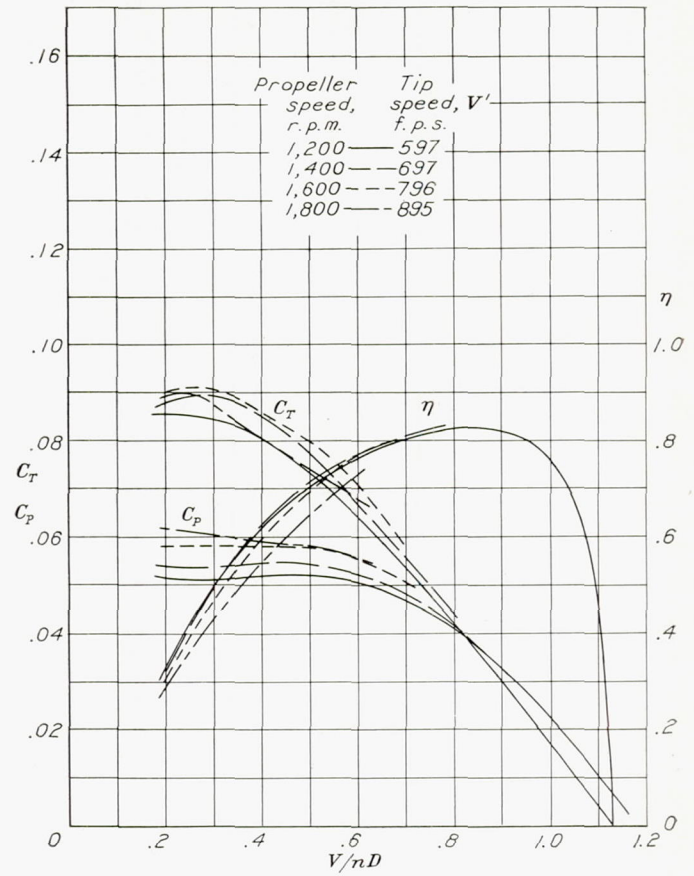
FIGURE 22.—Propeller set 15° at 0.75R.

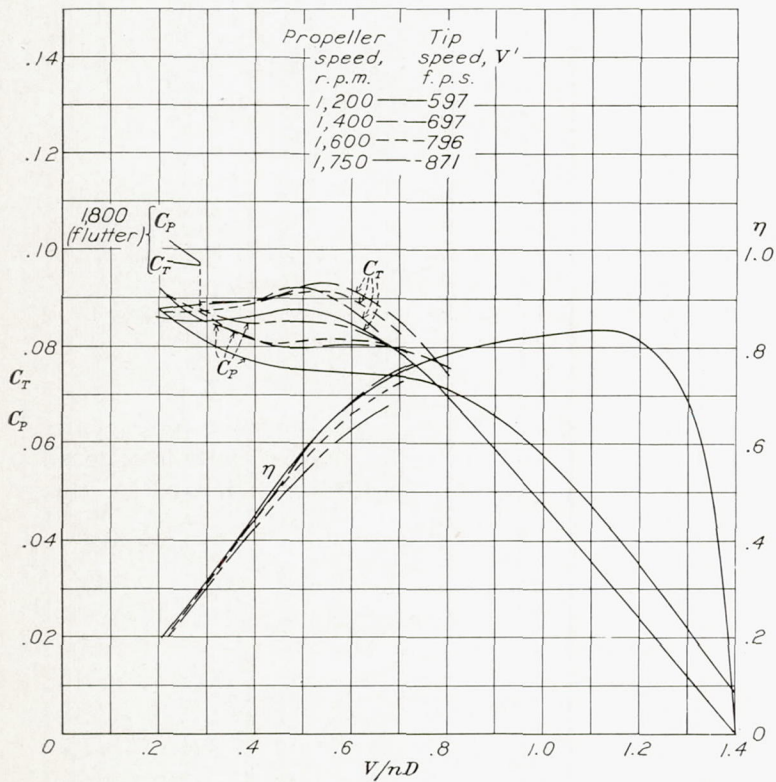FIGURE 23.—Propeller set 20° at 0.75R.
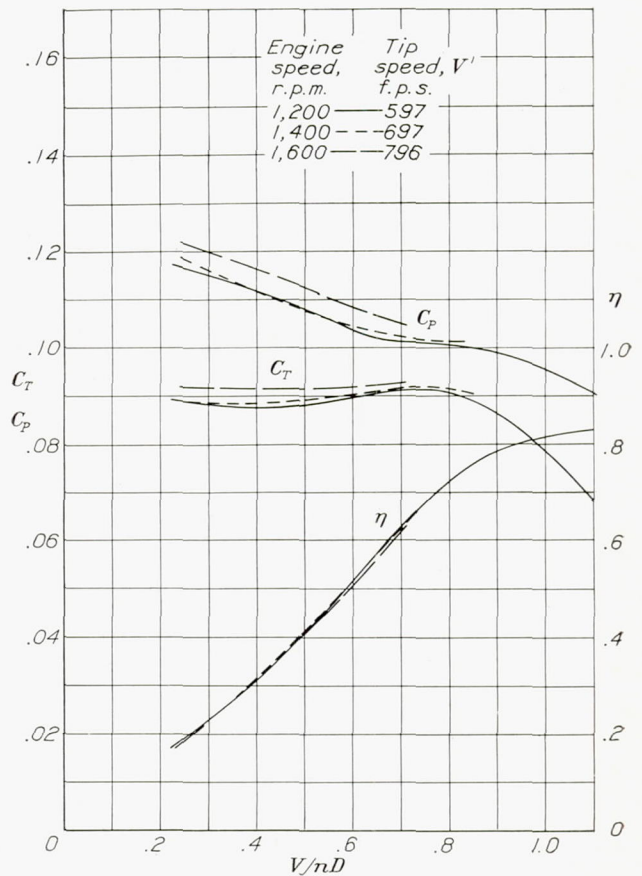

FIGURE 24.—Propeller set 25° at 0.75R.

FIGURE 25.—Propeller set 30° at 0.75R.

FIGURES 22 TO 25.—Effect of compressibility on propeller characteristics.   Propeller 4879; diameter, 9½ ft.; radial engine nacelle.

at high tip speeds, inasmuch as the efficiency at low tip speeds for the R. A. F. 6 propeller is greater than that for the Clark Y propeller in these ranges. (See figs. 9, 10, 16, and 17.)

A plausible explanation for the greater compressibility effect on the R. A. F. 6 propeller seems to lie in the differences of the radii of curvature of the front upper surfaces of the sections. (See fig. 7.) The R. A. F. 6 section has the lesser radius of curvature, hence the induced velocities are probably greater. The compressibility burble should therefore occur earlier for the R. A. F. 6 section.

shank portions of the blades, however, are nearly identical. A comparison of the results from these propellers (fig. 49) indicates that the compressibility loss for the wider blade is only about half that for the one of standard width in the take-off range. The differences are more obscure for the climbing condition. The actual efficiencies become nearly equal at high tip speeds, however, since the standard-width blade has a higher efficiency at low tip speeds. (See figs. 36, 37, 40, and 41.)

Just why the differences in Reynolds Number of the two sets of tests should account for the differences
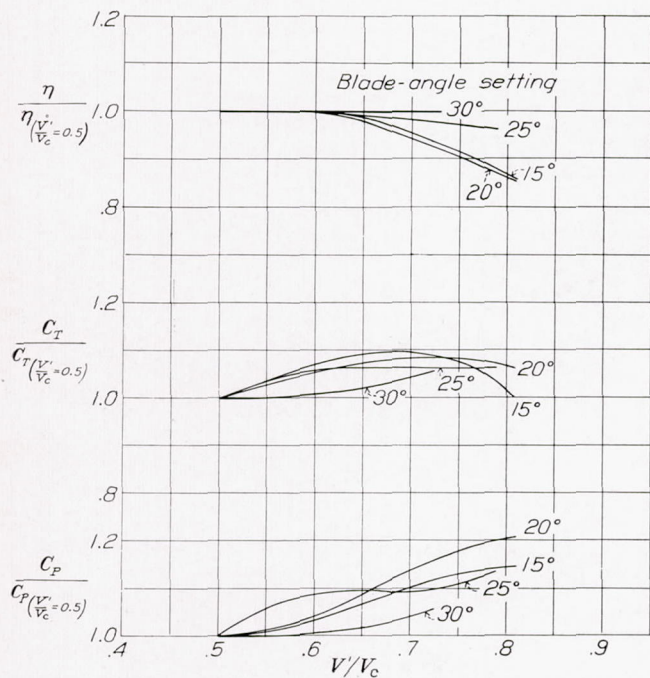

FIGURE 26.—Changes in propeller characteristics due to compressibility for the take-off condition. Propeller 4879; diameter, $9\frac{1}{2}$ ft.; radial engine nacelle; $\frac{V}{nD} = 0.30 \left(\frac{V}{nD} \right)_{peak\ eff.}$

FIGURE 27.—Changes in propeller characteristics due to compressibility for the climbing condition. Propeller 4879; diameter, $9\frac{1}{2}$ ft.; radial engine nacelle; $\frac{V}{nD} = 0.65 \left(\frac{V}{nD} \right)_{peak\ eff.}$

Blade shape.—In figure 48 is shown a comparison of three propellers having different blade shapes. The main difference is the tip shape, as can be seen from figure 3, although there are also differences in thickness. With the exception of the take-off comparison at a blade-angle setting of 20°, the results from the three propellers are almost identical.

Blade width.—Propeller 37–3647 is 50 percent wider than propeller 5868–R6, but otherwise the two propellers are identical. Since the thickness ratio is the same, the actual thickness of propeller 37–3647 is likewise 50 percent greater than that of propeller 5868–R6. The

noted is not clear. The wider blade produces a greater inflow velocity and, consequently, is working at a lower angle of attack than the standard-width one. The inflow angle could hardly be increased, however, by the amount necessary to make the difference shown at the take-off condition, equivalent to a 5° change in blade-angle setting, because the 15° curve of the standard-width blade coincides with the 20° curve of the wider blade. Computations based on the momentum theory, however, do indicate an inflow angle greater by 0.75°, owing to the increased blade width, for one condition investigated.

FIGURE 28.—Propeller set 15° at 0.75R.

FIGURE 29.—Propeller set 20° at 0.75R.

FIGURES 28 AND 29.—Effect of compressibility on propeller characteristics. Propeller 4371; diameter, 11 ft.; radial engine nacelle.

FIGURE 30.—Changes in propeller characteristics due to compressibility for the take-off condition. Propeller 4371; diameter, 11 ft.; radial engine nacelle; $\frac{V}{nD} = 0.30 \left(\frac{V}{nD}\right)_{peak\ eff.}$
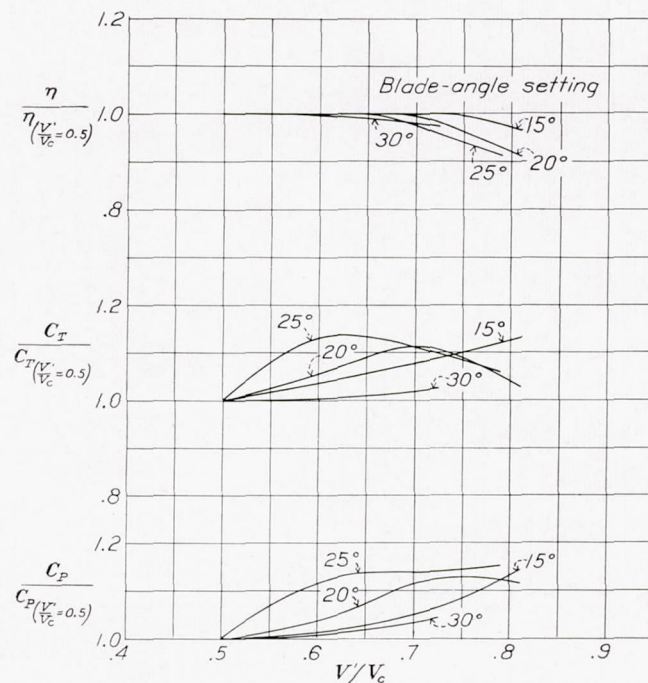
FIGURE 31.—Changes in propeller characteristics due to compressibility for the climbing condition. Propeller 4371; diameter, 11 ft.; radial engine nacelle, $\frac{V}{nD} = 0.65 \left(\frac{V}{nD}\right)_{peak\ eff.}$

FIGURE 32.—Propeller set 15° at 0.75R.

FIGURE 33.—Propeller set 20° at 0.75R.

FIGURES 32 AND 33.—Effect of compressibility on propeller characteristics. Propeller 195; diameter, 11 ft.; radial engine nacelle.
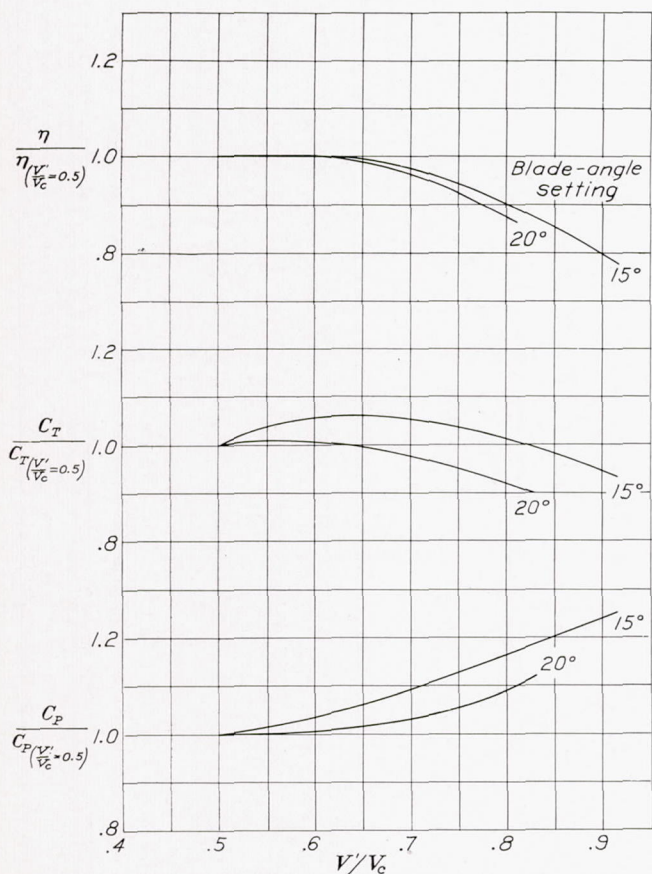
FIGURE 34.—Changes in propeller characteristics due to compressibility for the take-off condition. Propeller 195; diameter, 11 ft.; radial engine nacelle; $\frac{V}{nD}=0.30\left(\frac{V}{nD}\right)_{peak\ eff.}$

FIGURE 35.—Changes in propeller characteristics due to compressibility for the climbing condition. Propeller 195; diameter, 11 ft.; radial engine nacelle; $\frac{V}{nD}=0.65\left(\frac{V}{nD}\right)_{peak\ eff.}$
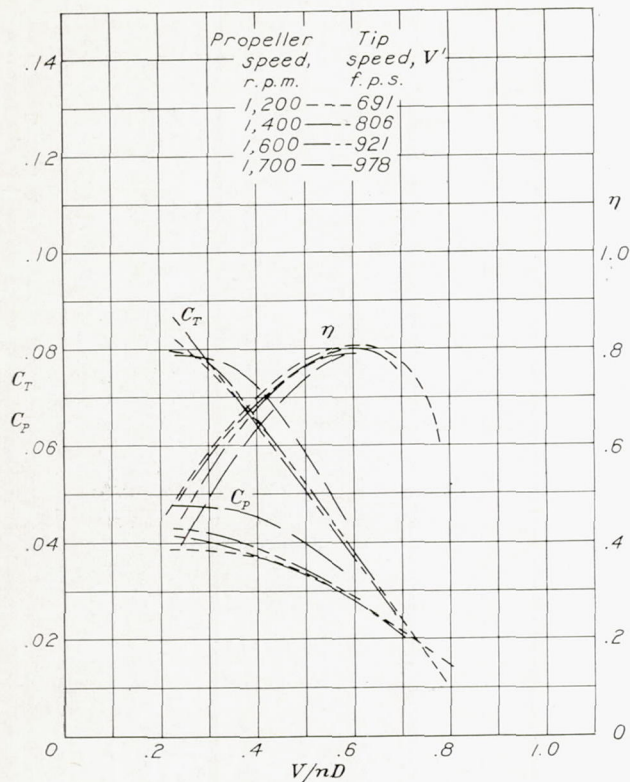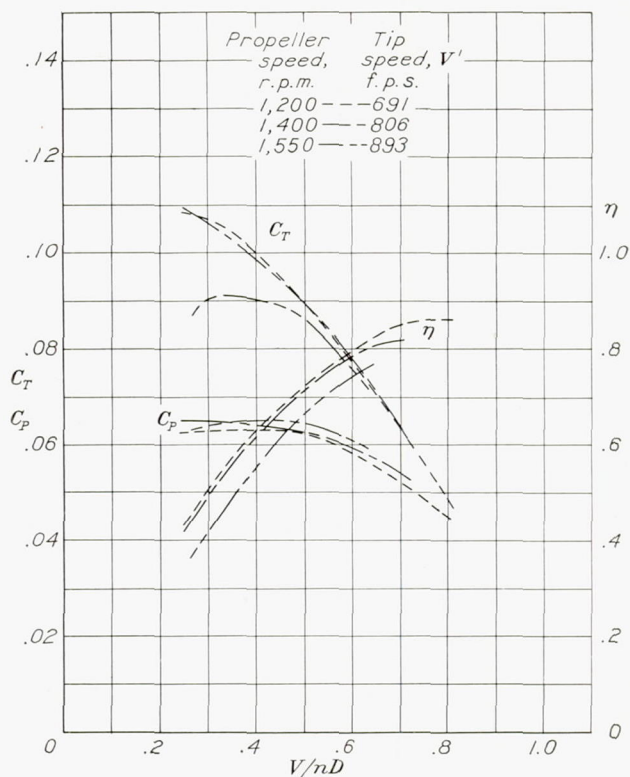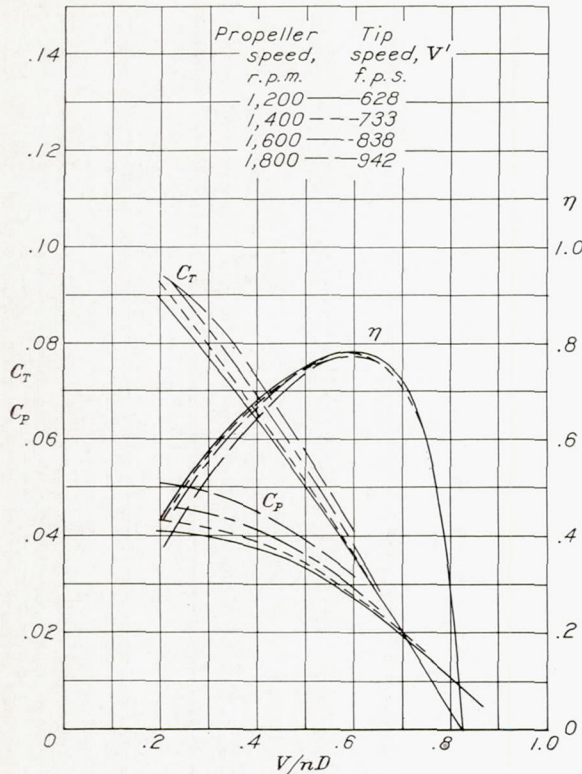
FIGURE 36.—Propeller set 15° at 0.75R.
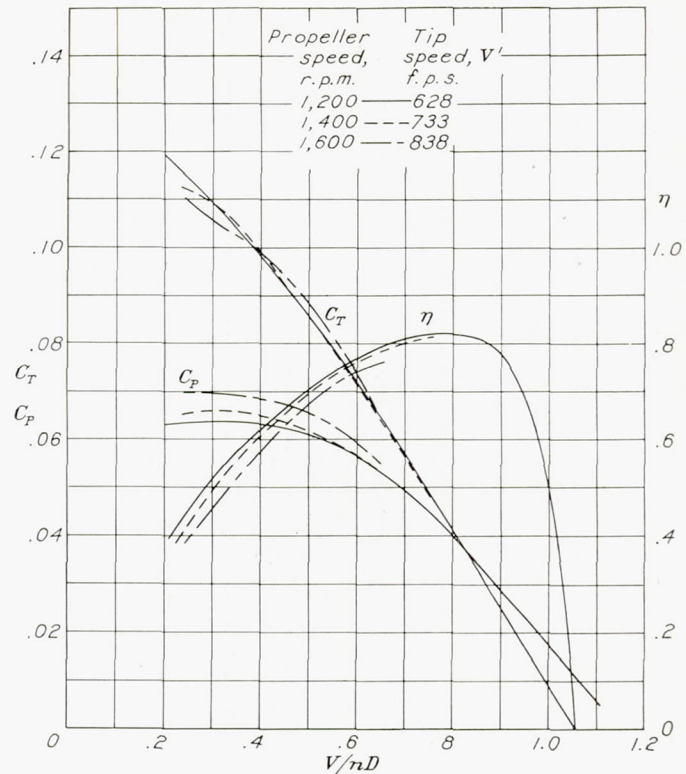
FIGURE 37.—Propeller set 20° at 0.75R.

FIGURES 36 and 37.—Effect of compressibility on propeller characteristics.   Propeller 5868–R6; diameter, 10 ft.; liquid-cooled engine nacelle.
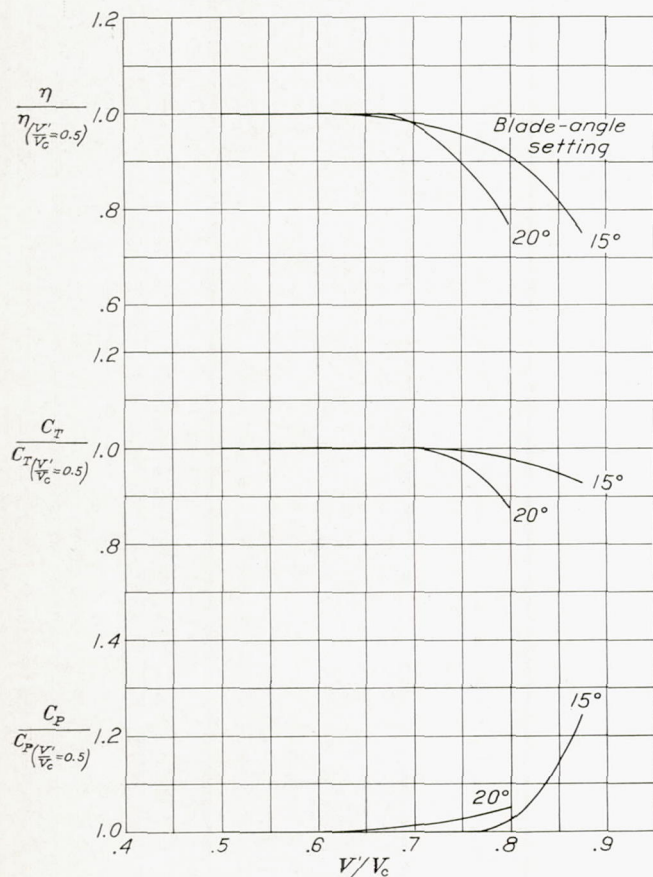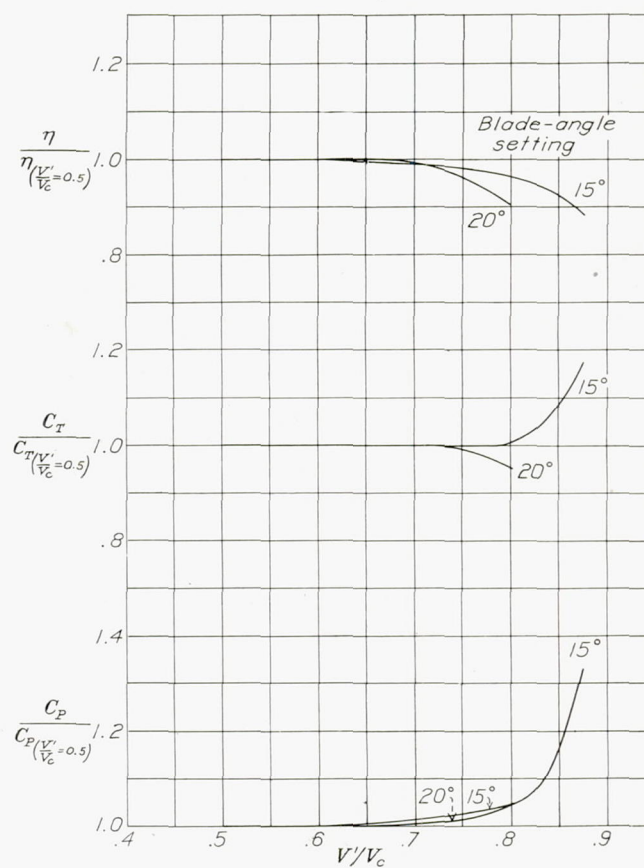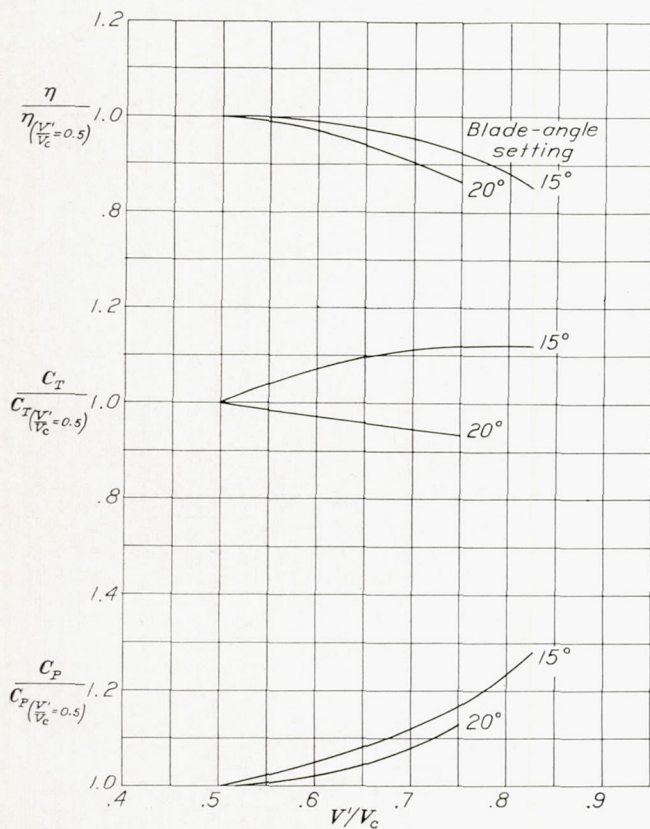

FIGURE 38.—Changes in propeller characteristics due to compressibility for the take-off condition. Propeller 5868–R6; diameter, 10 ft.; liquid-cooled engine nacelle;
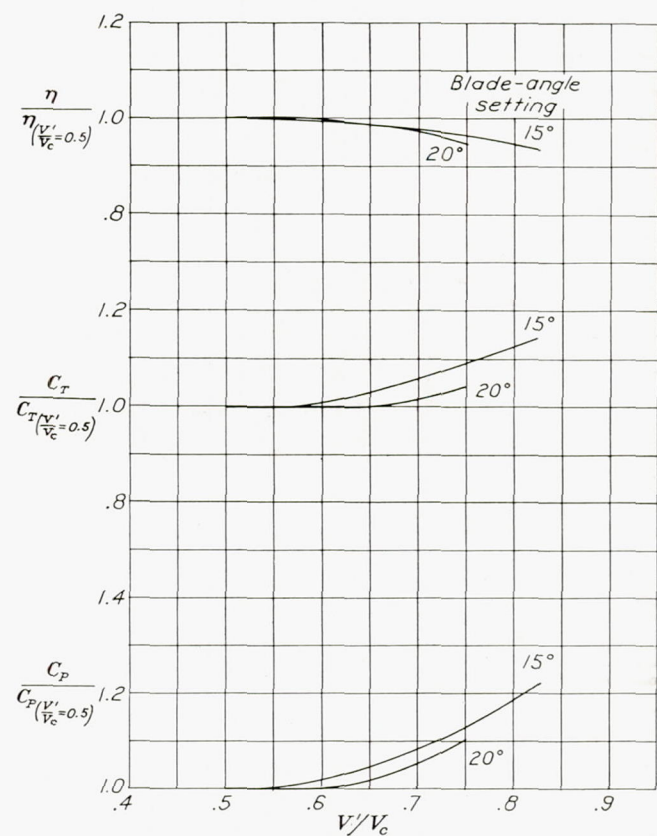
$$\frac{V}{nD}=0.30\left(\frac{V}{nD}\right)_{peak\ eff.}$$

FIGURE 39.—Changes in propeller characteristics due to compressibility for the climbing condition. Propeller 5868–R6; diameter, 10 ft.; liquid-cooled engine nacelle;

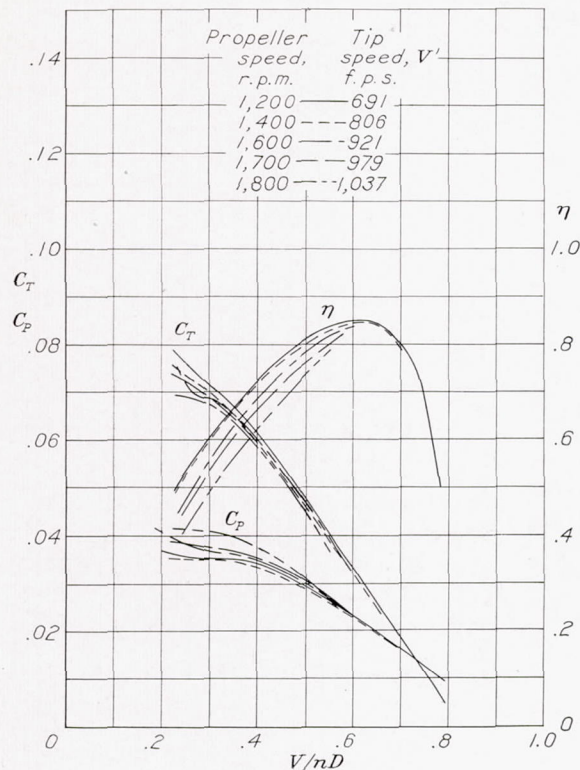$$\frac{V}{nD}=0.65\left(\frac{V}{nD}\right)_{peak\ eff.}$$
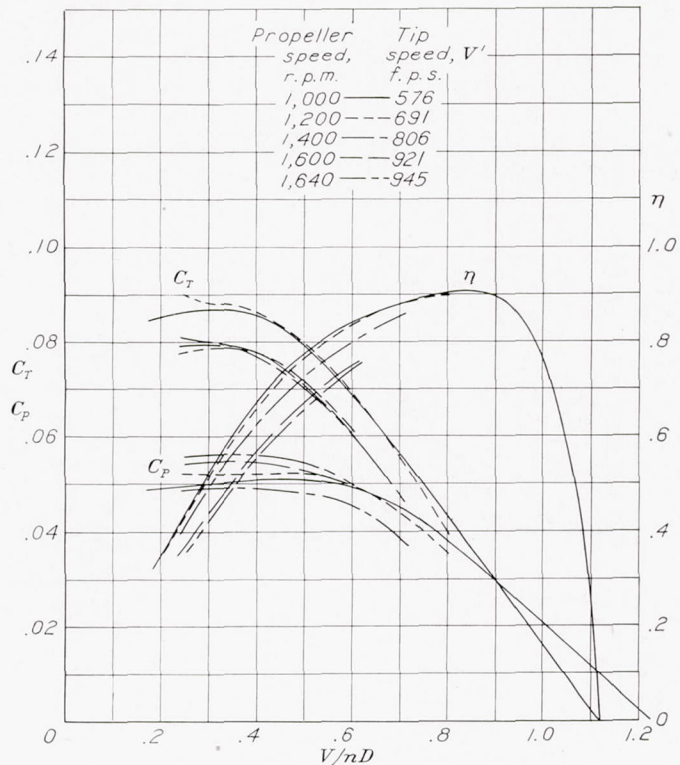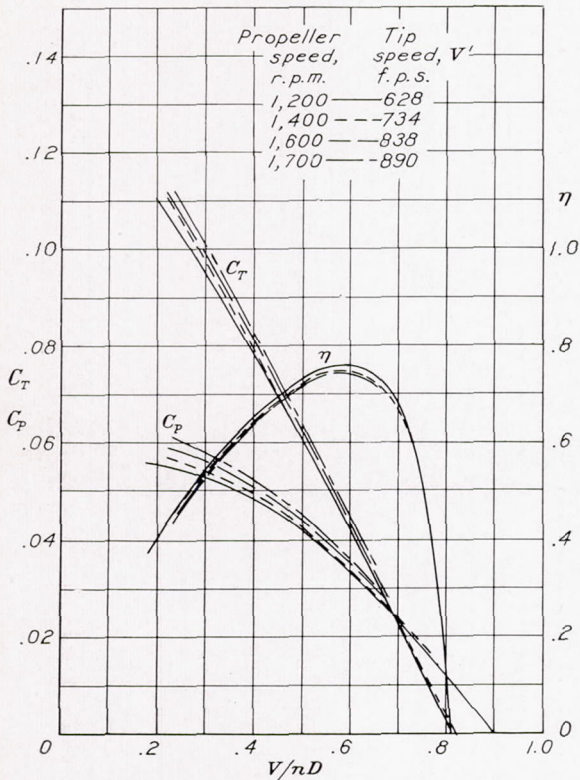
FIGURE 40.—Propeller set 15° at 0.75R.
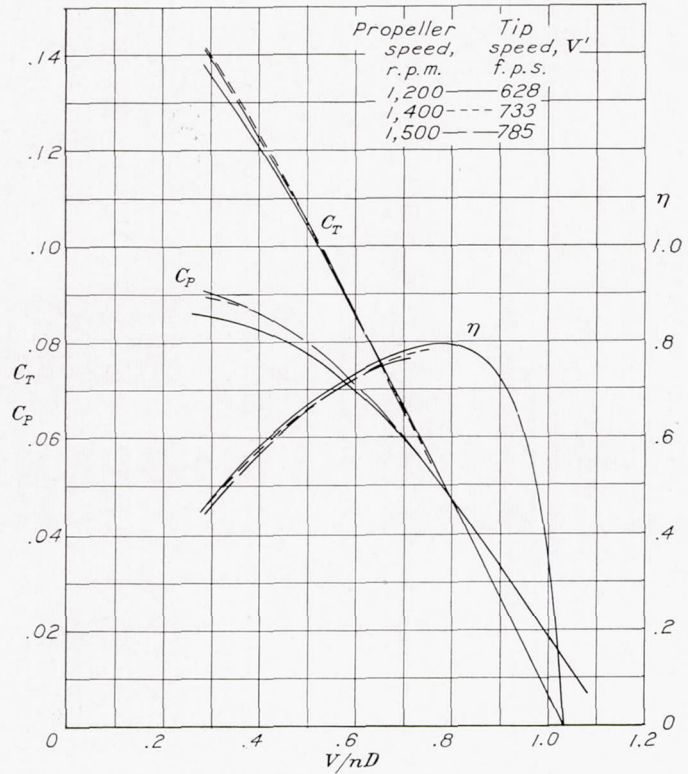
FIGURE 41.—Propeller set 20° at 0.75R.

FIGURES 40 and 41.—Effect of compressibility on propeller characteristics.   Propeller 37-3647; diameter, 10 ft.; liquid-cooled engine nacelle.
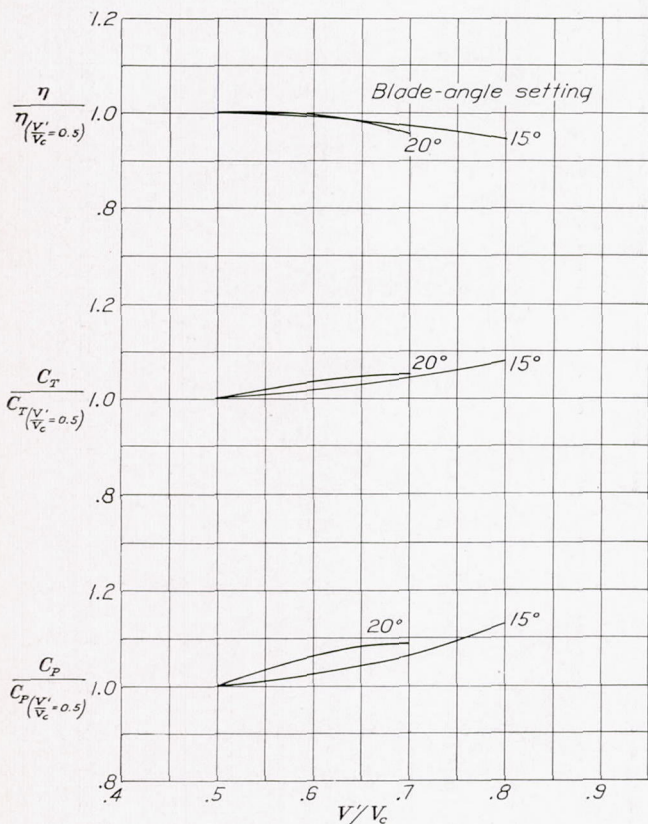
FIGURE 42.—Changes in propeller characteristics due to compressibility for the take-off condition. Propeller 37-3647; diameter, 10 ft.; liquid-cooled engine nacelle; $\frac{V}{nD} = 0.30 \left(\frac{V}{nD}\right)_{peak\ eff.}$
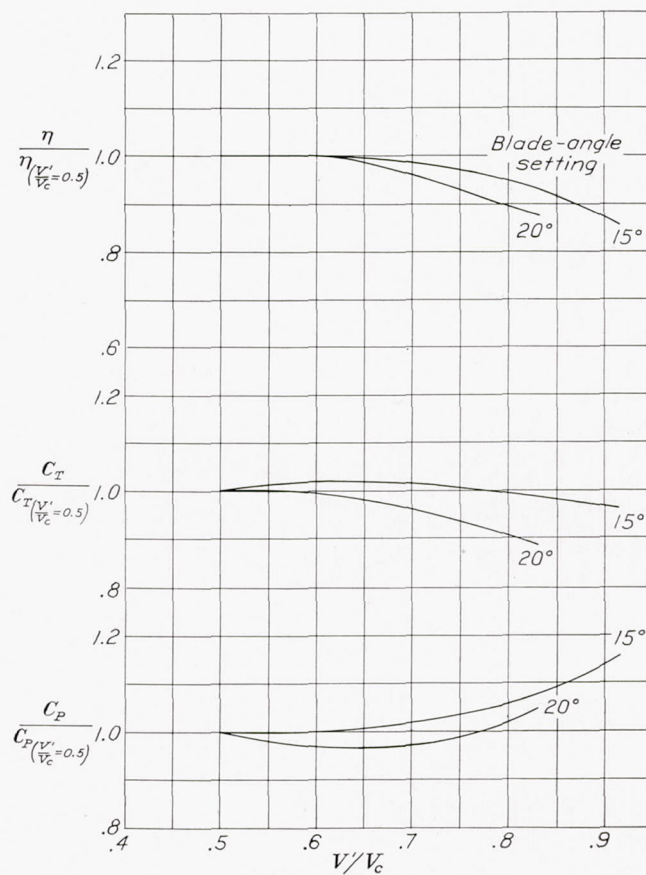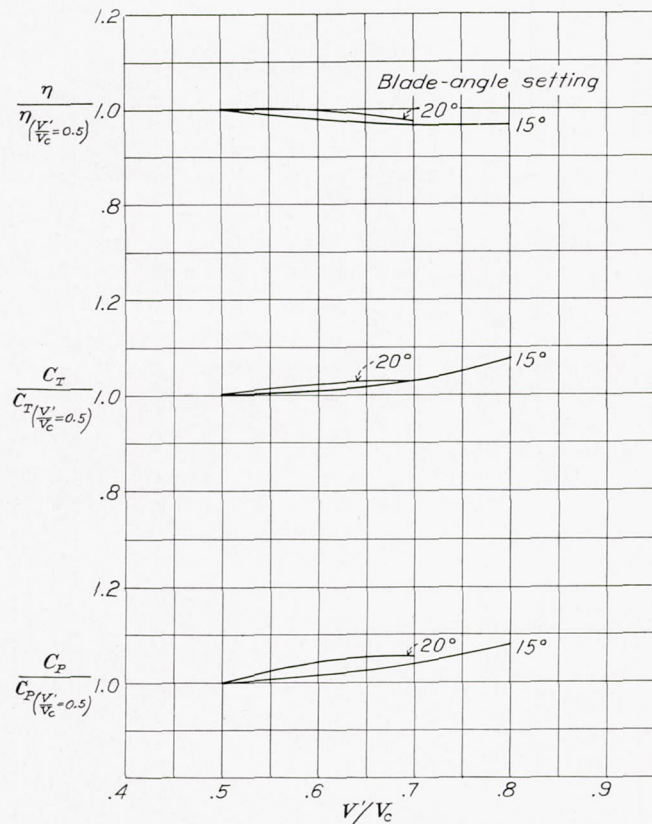

FIGURE 43.—Changes in propeller characteristics due to compressibility for the climbing condition. Propeller 37-3647; diameter, 10 ft.; liquid-cooled engine nacelle; $\frac{V}{nD} = 0.65 \left(\frac{V}{nD}\right)_{peak\ eff.}$
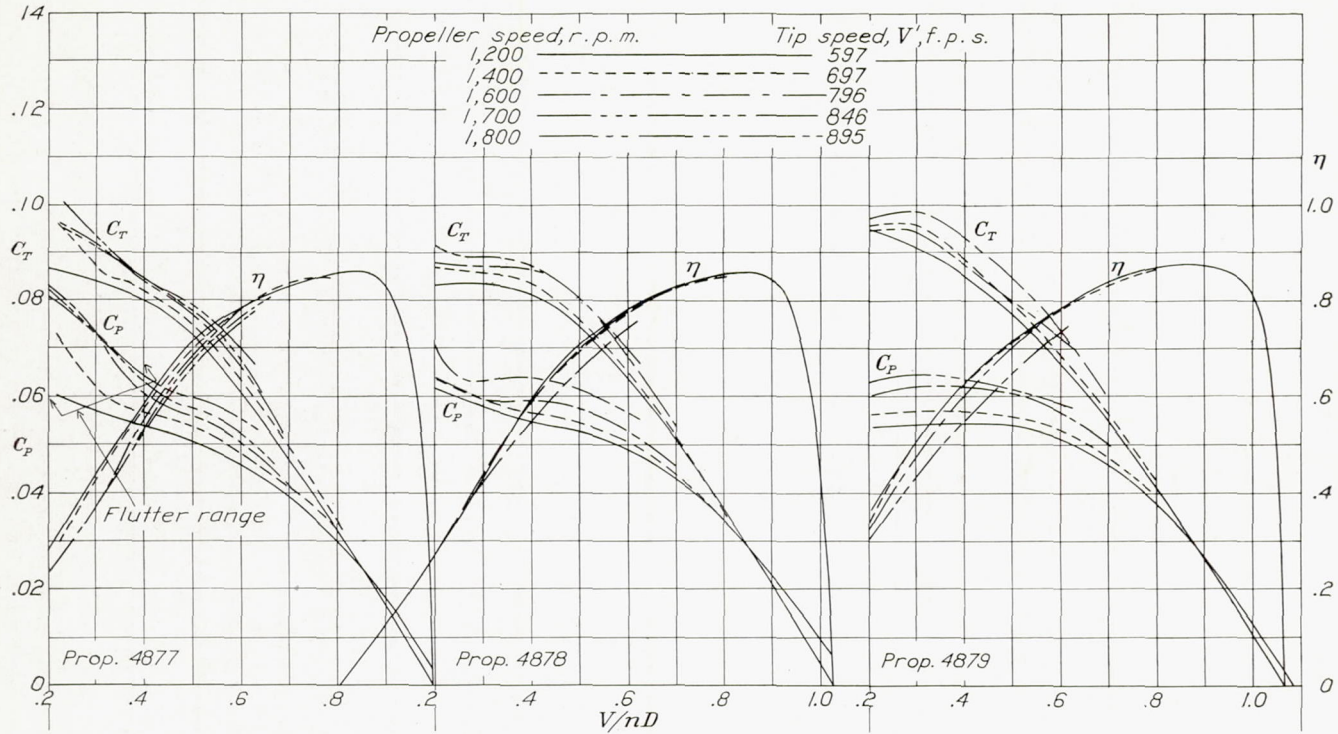
FIGURE 44.—Propeller 4877; $h/b=0.06$.   FIGURE 45.—Propeller 4878; $h/b=0.08$.   FIGURE 46.—Propeller 4879; $h/b=0.10$.

FIGURES 44, 45, and 46.—Effect of compressibility on propeller characteristics.   Propeller diameters, 9½ ft.; set 20° at $0.75R$; liquid-cooled engine nacelle.
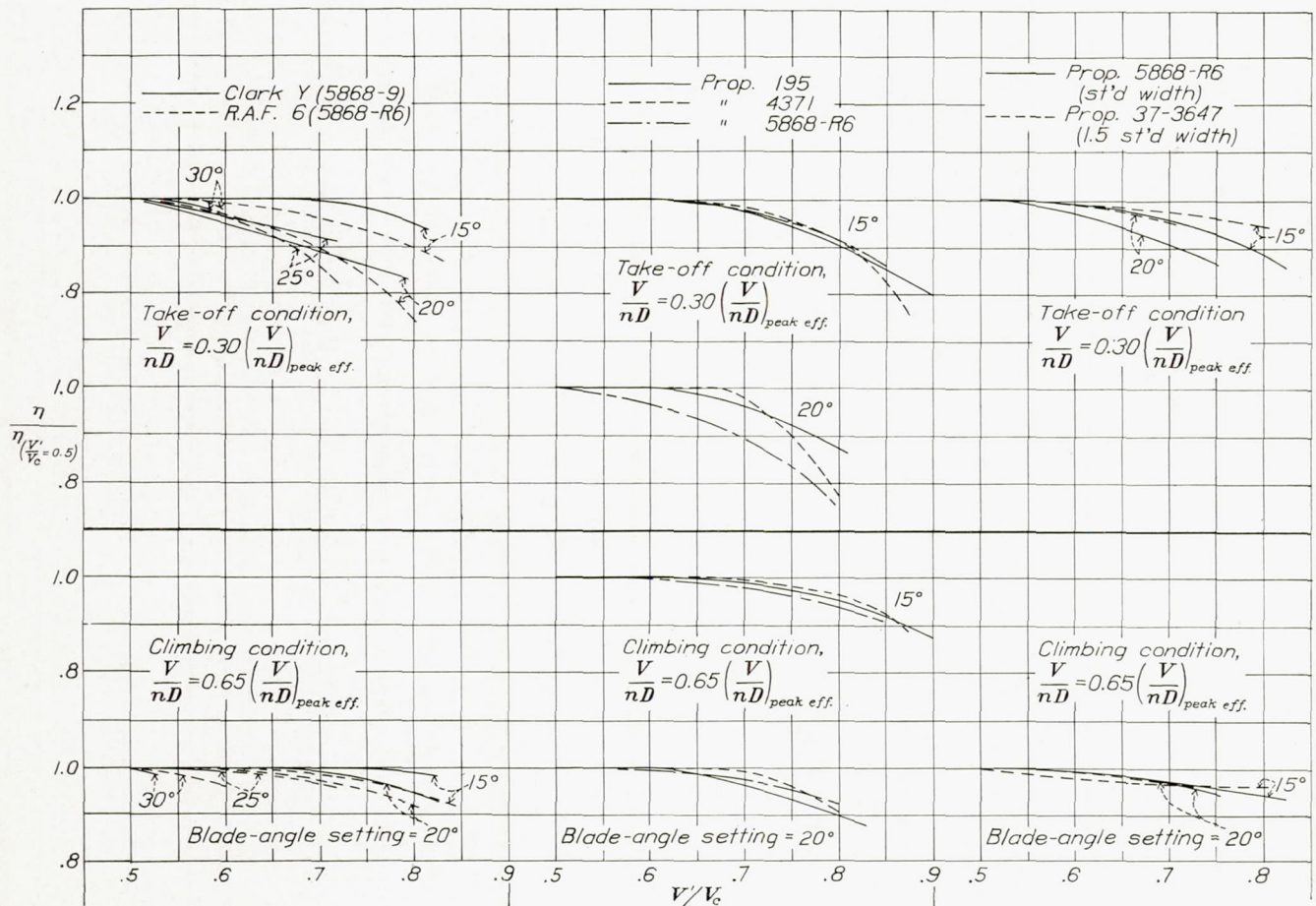
FIGURE 47.—Comparison of propellers having different sections.   FIGURE 48.—Comparison of three propellers having different blade shapes, R. A. F. 6 section.   FIGURE 49.—Comparison of propellers having different blade widths.   Liquid-cooled engine nacelle; R. A. F. 6 section.
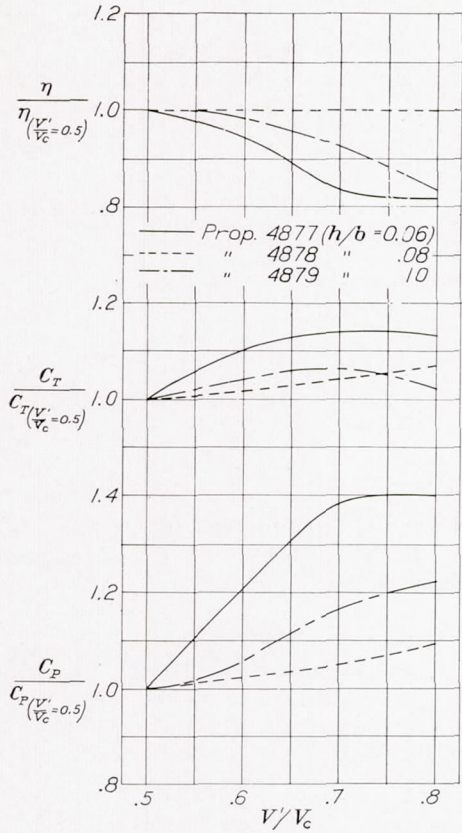
FIGURE 50.—Comparison of propellers having different blade thicknesses. Take-off condition; propeller set 20° at 0.75R; diameter, 9½ ft.; liquid-cooled engine nacelle;

$$\frac{V}{nD} = 0.30 \left(\frac{V}{nD}\right)_{peak\ eff.}$$

Propeller 4877 is fluttering at this condition.
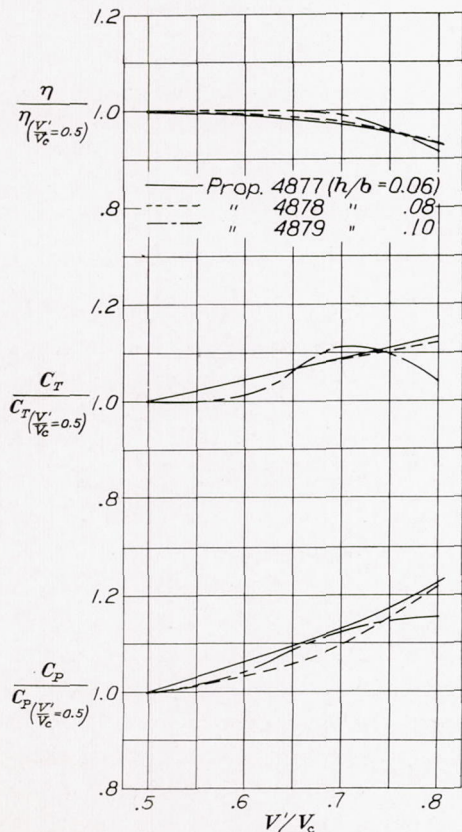
FIGURE 51.—Comparison of propellers having different blade thicknesses. Climbing condition; propeller set 20° at 0.75R; diameter, 9½ ft.; liquid-cooled engine nacelle;

$$\frac{V}{nD} = 0.65 \left(\frac{V}{nD}\right)_{peak\ eff.}$$
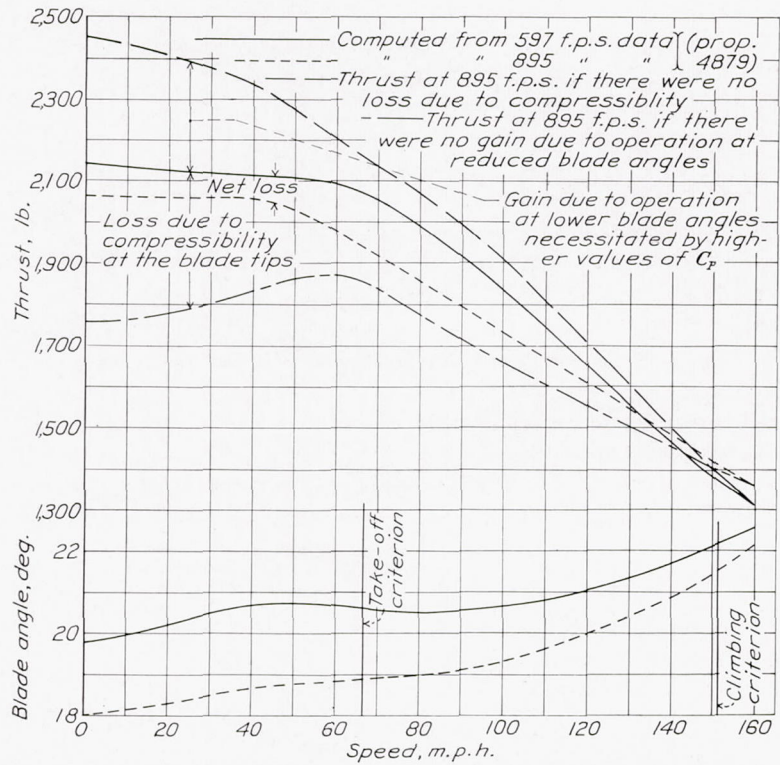
FIGURE 52.—Take-off and climbing thrust computed from low and high tip-speed data for a controllable propeller. Design conditions: 690 b. hp.; propeller speed, 1,500 r. p. m.; air speed, 224 m. p. h ; diameter, 11.35 ft.; C_P, 0.0542.
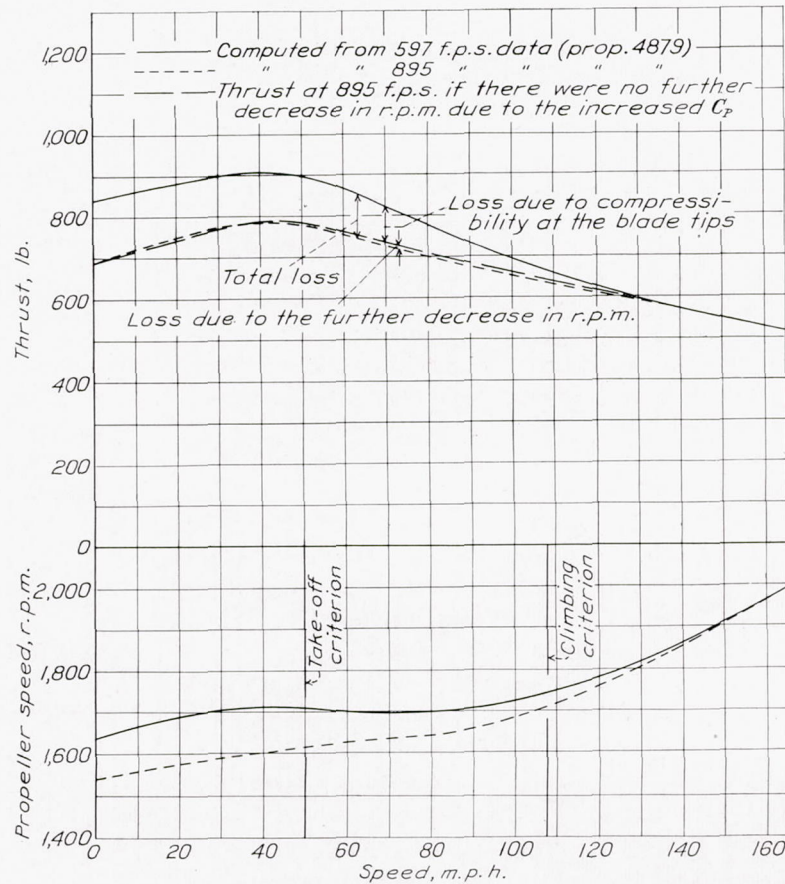
FIGURE 53.—Thrust computed from low and high tip-speed data for a fixed-pitch propeller. Design conditions: 285 b. hp.; propeller speed, 2,000 r. p. m.; air speed, 166 m. p. h.; diameter, 8.6 ft.; blade-angle setting, 20°.

Blade thickness.—Propellers 4877, 4878, and 4879 constitute a series differing only in thickness; they were built for the tip-speed experiments reported in reference 8. The tests reported herein were made at only one blade-angle setting, 20°; the results are given in figures 44, 45, and 46. Comparisons of the results from the three propellers are given in figures 50 and 51. During the tests it was noticed that the thinnest propeller (4877) fluttered violently at low air speeds, producing a very penetrating noise similar to that associated with supersonic tip speeds. The results very distinctly show the effect of flutter. In order to avoid confusing flutter effects with compressibility effects, the flutter effects will later be discussed as a separate topic.

If the results from propeller 4877 be neglected for the take-off condition on account of flutter, it appears that the thickest propeller (4879) is affected more by compressibility than the medium thick one; in fact, no loss

FIGURE 54.—Cross-faired thrust-coefficient curves. Propeller 4879; diameter, 9½ ft.; radial engine nacelle; propeller speed, 1,200 r. p. m.; tip speed, 597 f. p. s.

is evident for propeller 4878. It happens that the low tip-speed efficiency of the thick propeller (4879) is higher than that for propeller 4878, so their efficiencies at high tip speeds become nearly equal. (See figs. 45 and 46.) The results for the climbing condition are nearly identical for all three propellers.

Flutter.—The study of flutter does not come within the scope of this investigation. Flutter did exist, however, in some instances and the results were considerably affected thereby. As previously mentioned, propeller 4877 fluttered violently when operating at low air speeds. It may be noted from figure 44 that the power and the thrust were both increased by perhaps 10 or 20 percent, judging by the shape of the curves. There is no way of isolating compressibility and flutter effects except by assuming that breaks should not occur in the curves if flutter effects are absent. It is quite likely that most of the loss in efficiency observed in figure 50 is due to flutter, amounting to about 18 percent for tip speeds of $0.8V_c$.

An attempt was made to measure the amplitude of blade-torsional vibration of this propeller by the method of measuring blade deflection previously mentioned. The tests indicate that the blade at 0.75 radius was vibrating in torsion through an amplitude of between 1° and 2° when the propeller was turning at 1,600 r. p. m. The amplitude of the tip-section vibration was probably much greater.

EXAMPLES SHOWING THE EFFECT OF COMPRESSIBILITY ON THE TAKE-OFF AND CLIMBING THRUST OF CONTROLLABLE AND FIXED-PITCH PROPELLERS

Were it not for the fact that compressibility influences both the power absorption and the efficiency characteristics of propellers, it would be fairly easy to correct take-off and climbing computations for differences in tip speeds between propeller-test and airplane-operating conditions. The increased power coefficients associated with high tip speeds will necessitate lower blade-angle operation for controllable propellers and

FIGURE 55.—Cross-faired power-coefficient curves. Propeller 4879; diameter, 9½ ft.; radial engine nacelle; propeller speed, 1,200 r. p. m.; tip speed, 597 f. p. s.

the efficiency will be thereby increased; whereas, for the fixed-pitch propeller, the engine speed will be reduced for a given air speed, which affects both the brake horsepower and the propulsive efficiency. Specific examples have been worked out for both types of propeller (figs. 52 and 53) using data from propeller 4879 (radial engine nacelle). These data, which are cross-faired in figures 54 to 57, were used because a greater range of blade-angle settings and tip speeds was covered than with any other propeller.

Controllable propeller.—The example of the controllable propeller (see fig. 52) is based on a 690-horsepower engine turning a propeller at a speed of 1,500 r. p. m. The airplane speed is 224 miles per hour. Thrust curves at the take-off and climbing conditions

are computed from data for tip speeds of 597 and 895 feet per second.

These computations show, for this example, a loss of 5 or 6 percent in take-off thrust due to high tip speeds and show a slight gain at the climbing condition. This loss appears rather insignificant as compared with the 12 or 13 percent loss indicated in figure 26. Another factor, however, enters to explain the difference. The blade angle must be decreased about 2° on account of the higher power coefficients for the tip speed of 895 feet per second, with the result that the efficiency is increased and the over-all loss is thereby reduced.

In order to separate the actual loss due to compressibility from the effects due to changing the blade angle, a fictitious propeller was assumed that could have the blade width changed in order to maintain the power
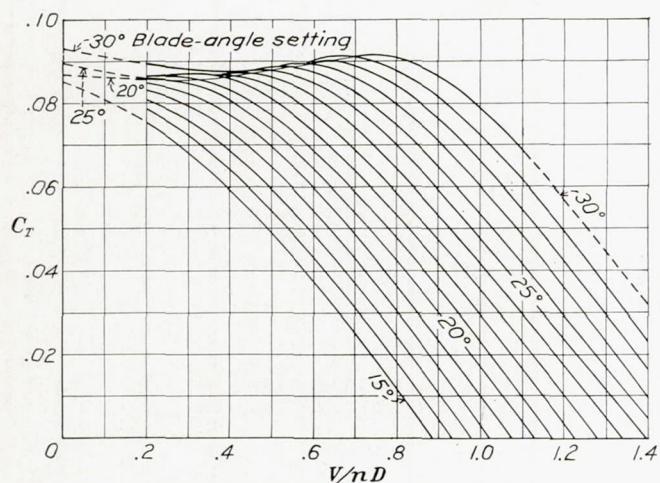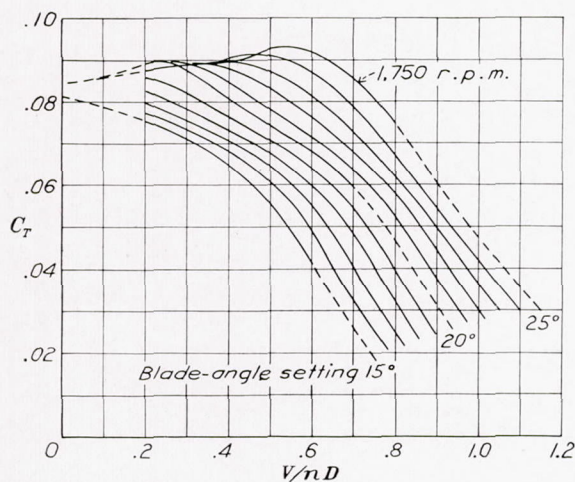

FIGURE 56.—Cross-faired thrust-coefficient curves. Propeller 4879; diameter, 9½ ft.; radial engine nacelle; propeller speed, 1,800 r. p. m.; tip speed, 895 f. p. s.

coefficient constant at the same blade angles as for the low tip-speed computation. The thrust is proportionately corrected for the change in blade width. This computation indicates a loss due to compressibility of from 10 to 18 percent in the take-off range. The curve showing the gain due to operating at lower blade angles is taken as the difference between the loss due to compressibility and the net loss.

Fixed-pitch propeller.—The example of the fixed-pitch propeller was worked out for different conditions from the previous example because a design blade-angle setting of 20° was desired. A 285-horsepower engine turning the propeller at 2,000 r. p. m. and a high speed of 166 miles per hour were assumed.

A total loss of about 13 percent is indicated (fig. 53) for the take-off condition and about 4 percent for the climb. A small part of this loss is due to the lowered engine speed brought about by the higher power coefficients of the data for 895 feet per second. A reduction in engine speed reduces the brake horsepower,

but the propulsive efficiency is increased for a given air speed owing to the higher operating V/nD. The net loss due to lowered engine speed is small for this example but would have been more had the slope of the take-off thrust curves been steeper.

This example does not give a true picture of the compressibility effects for a particular case because the tip speed was assumed to remain constant even though the propeller speed decreased. The example does give a true picture of the effects of compressibility at any particular air speed if it is assumed that the tip speed is 895 feet per second.

A METHOD OF CORRECTING PROPELLERS FOR THE EFFECT OF COMPRESSIBILITY

A simplified method for correcting propellers for the effect of compressibility is given in the appendix of this report. The method is based on generalized correction factors that were derived from data presented in the report. The use of the correction factors makes it possible to correct, in a few minutes, the thrust of similar propellers for the effect of compressibility.
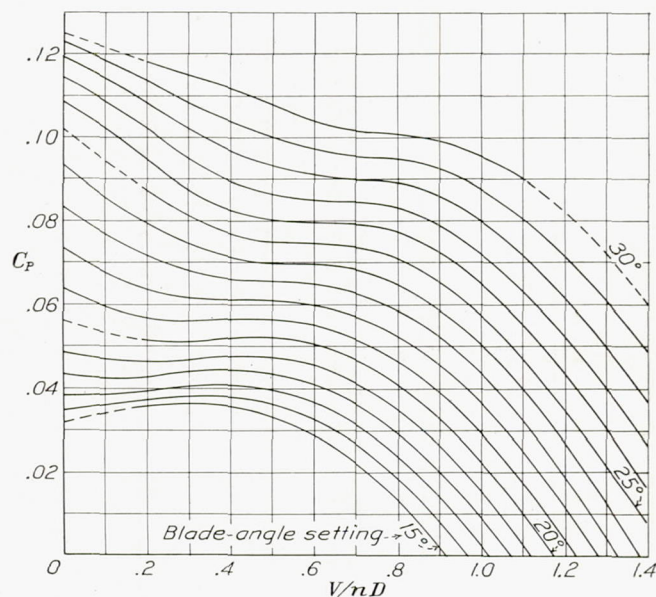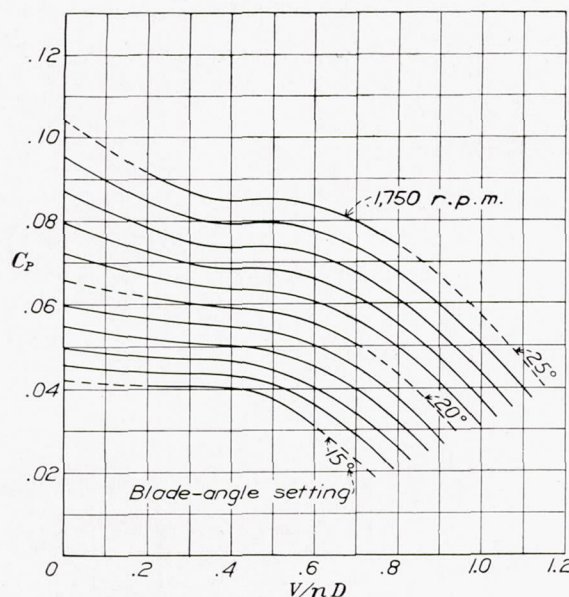

FIGURE 57.—Cross-faired power-coefficient curves. Propeller 4879; diameter, 9½ ft.; radial engine nacelle; propeller speed, 1,800 r. p. m.; tip speed, 895 f. p. s.

CONCLUDING REMARKS

The results of the tests indicate the following conclusions regarding the effect of tip speed:

1. Losses in propulsive efficiency due to compressibility became evident at from 0.5 to 0.7 the velocity of sound for the take-off and climbing conditions of flight, depending upon the propeller shape and the blade-angle setting. As the tip speed increased beyond these values the loss increased rapidly, amounting to more than 20 percent of the thrust power in some instances for tip-speed values of 0.8 the speed of sound.

2. The loss for the take-off condition increased with blade-angle setting up to a value of about 20° for a given tip-speed value. At higher blade angles the loss diminished.

3. The loss for the climbing condition increased with blade-angle setting for a given tip speed up to a value of about 25°, beyond which it decreased. Also, the losses appeared at lower tip speeds as the blade angle was increased.

4. Compressibility affected the propeller of R. A. F. 6 section to a greater extent than it did the propeller of Clark Y section; but, since the R. A. F. 6 propeller had a higher take-off efficiency at low tip speeds, the efficiencies nearly equalized at high tip speeds.

5. Compressibility affected standard-width blades to a greater extent than it did extremely wide blades for the take-off condition; but, since the standard-width blades had a higher efficiency at low tip speeds, the efficiencies nearly equalized at high tip speeds. The standard-width blades had an even higher efficiency at high tip speeds for the climbing condition.

6. The loss for the take-off condition due to compressibility was greater for a thick propeller than for a thin one; but, since the thick propeller had a higher efficiency at low tip speeds, the efficiency nearly equalized at high tip speeds. The effect of thickness was negligible for the climbing condition.

7. There was a marked tendency for the thrust and power coefficients to increase with tip speed, even before any loss in the efficiency was detected.

8. The loss in efficiency for controllable propellers due to compressibility was partly regained by the lower blade-angle operation necessitated by the higher power coefficients.

9. The loss in efficiency for fixed-pitch propellers due to compressibility was further increased by a loss in engine speed and power caused by the higher power coefficients.

10. Comparisons of propellers having different blade sections, blade widths, and blade thicknesses, made on the basis of data for propellers operating at low tip speeds, are likely to be misleading, inasmuch as compressibility effects appreciably modify and, in many cases, tend to equalize any differences noted at the low V/nD range of operation.

APPENDIX

A METHOD OF CORRECTING PROPELLER CHARACTERISTICS FOR THE EFFECT OF COMPRESSIBILITY AT TIP SPEEDS BELOW 0.9 THE SPEED OF SOUND

The material presented in the body of the present report is not in a form convenient to use in correcting low-tip-speed propeller characteristics for compressibility effects encountered when operating at high tip speeds. The data are given in a basic form and additional curves are included to show certain trends. In order to make practical use of the material, it is necessary to devise a method whereby the characteristics of any propeller can be readily corrected for compressibility effects with reasonable certainty.

A number of factors associated with the problem make it extremely difficult, if not impossible, to devise any set of formulas or curves by which the characteristics of any propeller may be corrected. Differences in blade section, width, thickness, plan form, and pitch distribution account for differences in compressibility effects, so it is considered advisable to confine the correction factors to specific propellers, at least for the present. When sufficient data are accumulated, it may be possible to formulate a more generalized method that can be applied to any propeller, regardless of shape.

The present method of correcting propeller characteristics for compressibility effects is based on correction factors applied to the thrust and torque coefficients of either fixed-pitch or controllable propellers. The correction factors are presented in curve form for several propellers in figures 58 to 61. It is pointed out in the present report and elsewhere that the angle of attack of a blade element, or the lift coefficient, is a major parameter determining the magnitude of compressibility effects. Neither the angle of attack nor the lift coefficient can be readily determined for propellers but, inasmuch as the thrust coefficient of the propeller is closely related to the lift coefficients of the sections, the thrust coefficient is considered to be a good substitute. Through the use of the thrust coefficient as a correction parameter, the blade angle and V/nD are dispensed with so that the method is generalized to the extent that it can be applied to any blade-angle setting with reasonable accuracy.

The use of the thrust coefficient as a correction parameter has other advantages. Propellers having different numbers of blades may be corrected without additional considerations because the thrust coefficient at the stall is nearly proportional to the number of blades.

The normal stall of a propeller is readily apparent; the thrust-coefficient curves break in much the same manner as do lift-coefficient curves for airfoils. The flow over the airfoil sections changes; the peak of the negative pressures is eliminated and the corresponding induced velocities are materially reduced with the result that the effect of compressibility is greatly modified and uncertain. For this reason, the propeller correction factor used for the unstalled portion of the operating range should not be used for the stalled portion. The use of the thrust coefficient as a correction parameter draws attention to the operating range.

The correction factors given in figures 58 to 61 are in the form of ratios of C_T, C_P, and η at high tip speeds to those at low tip speeds (taken at approximately 0.5 the speed of sound). Individual curves are given for constant values of $C_T/C_{T(at\ stall)}$. These correction curves were obtained by plotting the data given in the body of the report and cross-fairing the resulting curves. It may be noted that the curves have been extrapolated from approximately 0.8 or 0.85 to 0.9 the speed of sound, in order to make the method more useful; consequently, these portions of the curves may be subject to some error.

USE OF THE CORRECTION FACTORS

Controllable propellers.—The power coefficient for operation is determined by the air density, the engine power, the propeller diameter, and the rotational speed. In view of the fact that the power coefficient increases with tip speed, it is necessary first to determine the values corresponding to the low-speed data because from these data the blade angles and the thrust are determined. These values are determined by dividing the design power coefficient by the ratios of the high-tip-speed to low-tip-speed power coefficients corresponding to the appropriate values of thrust coefficient and then by reading the blade angles and low-tip-speed thrust coefficients from the propeller curves. It is then necessary only to correct the coefficients for the effect of compressibility by the use of the factors to establish the operating values.
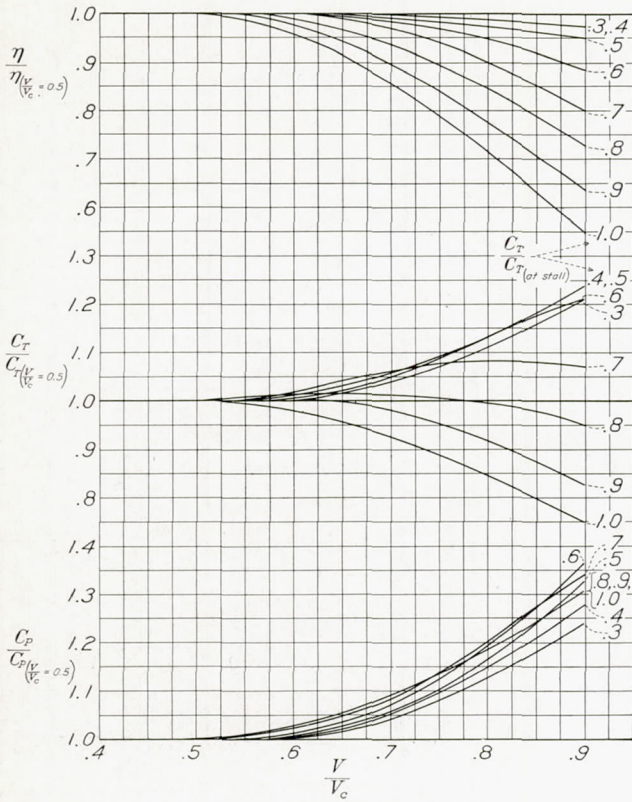
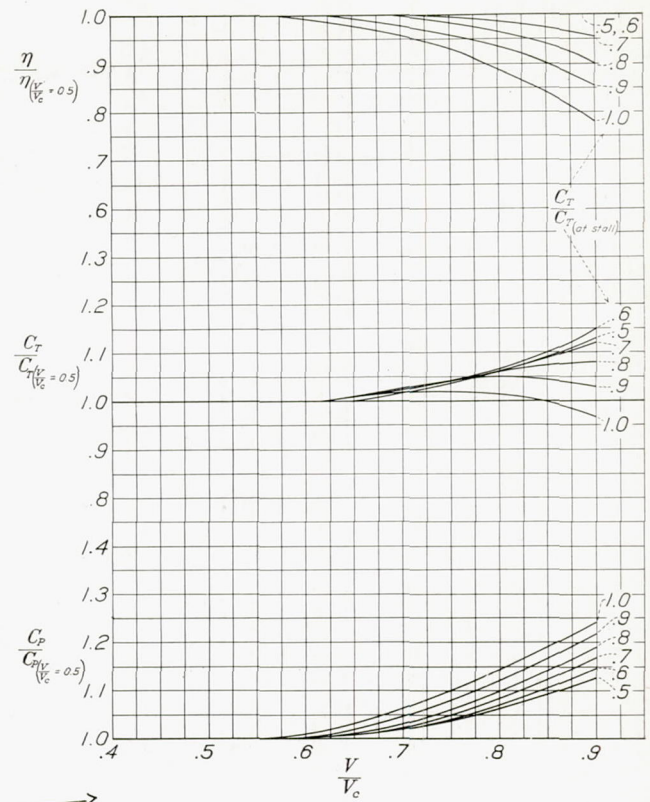FIGURE 58.—Correction factors for propeller 5868–9.

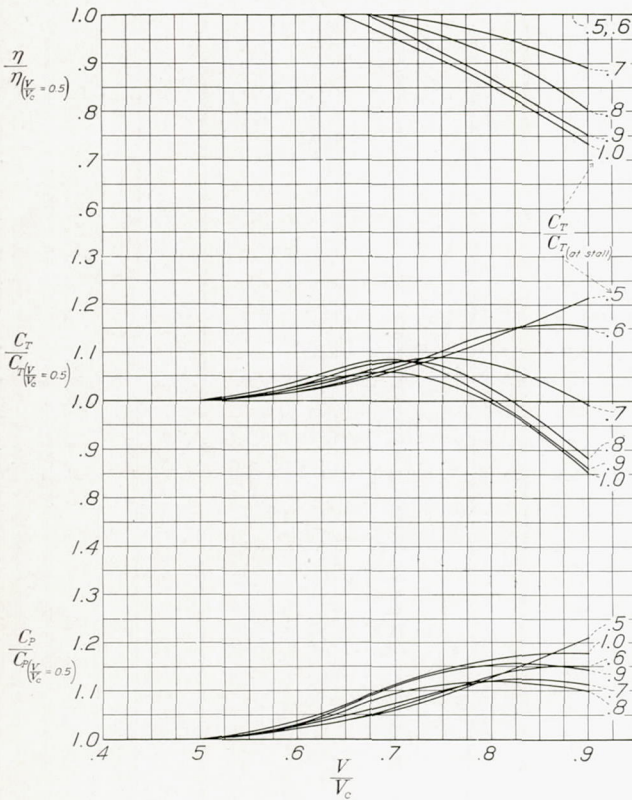FIGURE 59.—Correction factors for propeller 5868–R6.

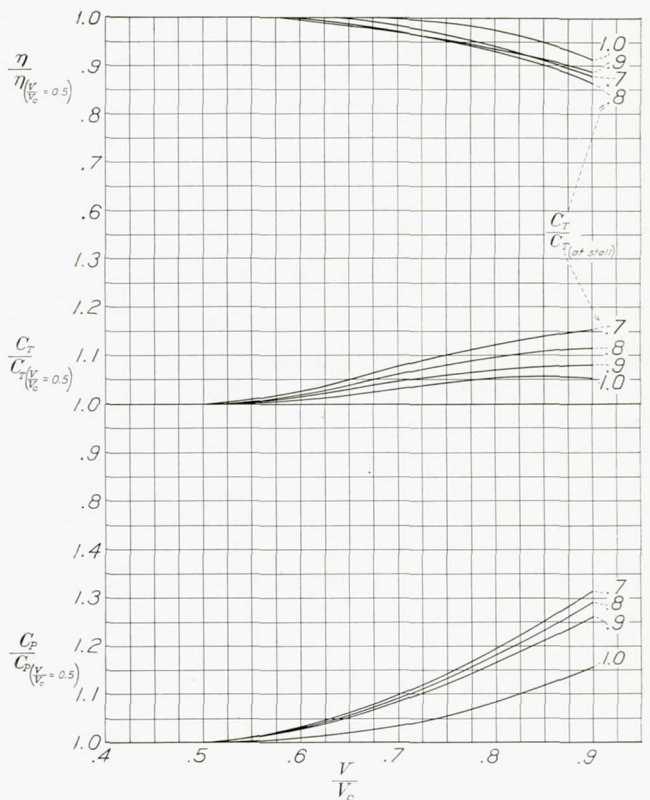FIGURE 60.—Correction factors for propeller 4879.

FIGURE 61.—Correction factors for propellers 4877 and 4878.

Several examples have been worked to illustrate the process and, at the same time, to show the magnitude of the compressibility effects for typical airplane installations. Example 1 is a check upon the method for controllable propellers presented in the body of the report. The computations are given in table I (a) and the final curves are shown in figure 62. The following series of operations is completed after the propeller has been designed or selected in the usual manner. (See table I (a).)

1. In column 1, values of V/nD are assumed.

2. The blades angle β_1 is read from the power-coefficient curves at low tip speeds (fig. 55) corresponding to the design C_{P_1} of 0.0542.

3. The thrust coefficient C_{T_1} is read from figure 54 for different values of β_1.

4. $C_{T_1}/C_{T(at\ stall)}$ is computed from the values given in column 3. The value of C_T at the stall is taken as .0 86. A high degree of accuracy is not necessary because the results are not used directly in the computations.

5. Power correction factors are read from figure 60 for values of $C_{T_1}/C_{T(at\ stall)}$ given in column 4 and for a value of V/V_c of 0.8.

6. The design power coefficient, $C_{P_1}=0.0542$, is

divided by the ratio $\dfrac{C_P}{C_{P\left(\frac{V}{V_c}=0.5\right)}}=\dfrac{C_{P_1}}{C_{P_2}}$ given in column

5 in order to determine the corresponding power coefficient C_{P_2} for the low-tip-speed data being used.

7. The blade angle β_2 corresponding to C_{P_2} is read from figure 55.

8. The thrust coefficient C_{T_2} corresponding to β_2 is read from figure 54.

At this stage of the correction the low-tip-speed data are fitted to the design requirements of the engine and propeller. It is now necessary to correct the thrust data for the higher tip speed of operation, namely $0.8V_c$.

9. The correction factor $\dfrac{C_T}{C_{T\left(\frac{V}{V_c}=0.5\right)}}=\dfrac{C_{T_3}}{C_{T_2}}$ is read

from figure 60 for values of $\dfrac{C_{T_1}}{C_{T(at\ stall)}}$ given in column

4 and a value of V/V_c of 0.8.

10. The corrected thrust coefficient C_{T_3} is obtained by multiplying C_{T_2} by the ratio C_{T_3}/C_{T_2} given in column 9.

11. The corrected thrust is obtained by multiplying C_{T_3} by the constant $\rho n^2 D^4$.

12. The air speed in miles per hour is obtained by

multiplying the V/nD given in column 1 by the constant $ND/88$, where N is the propeller rotational speed in r. p. m.

No computation is made for the correction of the low-speed power coefficient C_{P_2} because it is obvious that multiplying C_{P_2} by C_{P_1}/C_{P_2} results in C_{P_1}, the design power coefficient. It may be noted that the computations were carried through for the stalled portion of the operating range even though the method strictly should not be applied there. The error in this case is probably small since there is no evidence from any of the data that a sudden change in the effects of compressibility occurs at the stall.

From figure 62 it may be noted that the curve for the thrust, corrected by means of the charts, checks the thrust curve computed from the 895-feet-per-second data only for the low-speed range. The disagreement at the climbing part of the range is attributed to the fact that the charts are derived by averaging all the available data for this propeller; whereas the 895-feet-per-second curve is determined essentially by the one test at 20° blade angle, which was extrapolated for V/nD values higher than 0.7. Since the thrust curve derived by the chart method is based on more test points, it is considered to be the more accurate of the two.

In example 2, a 3-blade 5868–9 propeller is selected from the data given in reference 10 for a radial engine nacelle, and the thrust is corrected by the present method.

Given—

Engine_____ 1,000 horsepower.
Engine speed_____ 2,375 r. p. m., sea-level operation.
Air speed_____ 283 m. p. h.

Selection of the propeller—Design A:

$$C_s=\frac{0.638\times\text{m. p. h.}}{\text{hp.}^{1/5}\times N^{2/5}}=\frac{0.638\times283}{3.98\times22.35}=2.03$$

From figure 13 of reference 10,

$$\frac{V}{nD}=1.3$$

$$\eta=0.86$$

Then

$$D=\frac{88\times\text{m. p. h.}}{N\left(\dfrac{V}{nD}\right)_{design}}=\frac{88\times283}{2,375\times1.3}=8.06\ \text{ft.}$$

Tip speed at zero forward speed is 1,000 f. p. s.
Sound speed for standard conditions is 1,120 f. p. s.

$$\frac{V}{V_c}=0.895$$

$$C_{P(design)}=\frac{\text{hp.}\times550}{\rho n^3 D^5}=0.1097$$

Computation of thrust and correction for compressibility effects:

Table I (b), identical in form to table I (a), is filled in, using data taken from figure 10 of reference 10 and figure 58 of the present report. The corrected thrust and blade angles are plotted in figure 62, along with the

Any errors incidental to this extrapolation will have a negligible effect on the take-off run, provided that correct thrust values are obtained over the latter part of the take-off run.

It should be pointed out that the propeller of design A was selected from a C_s chart derived from low-tip-speed
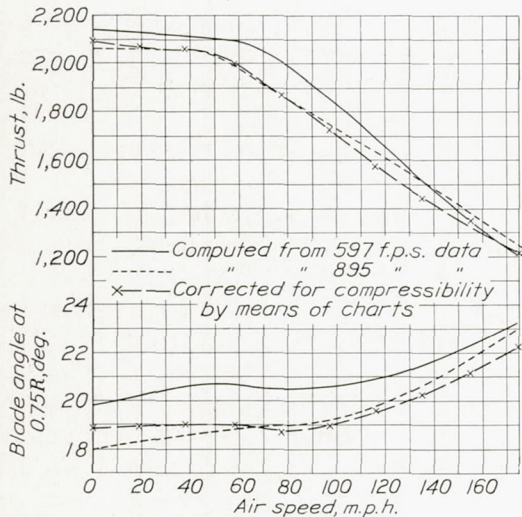
FIGURE 62.—Example 1 showing the uncorrected and corrected thrust and blade angles for an airplane equipped with propeller 4879 (controllable).
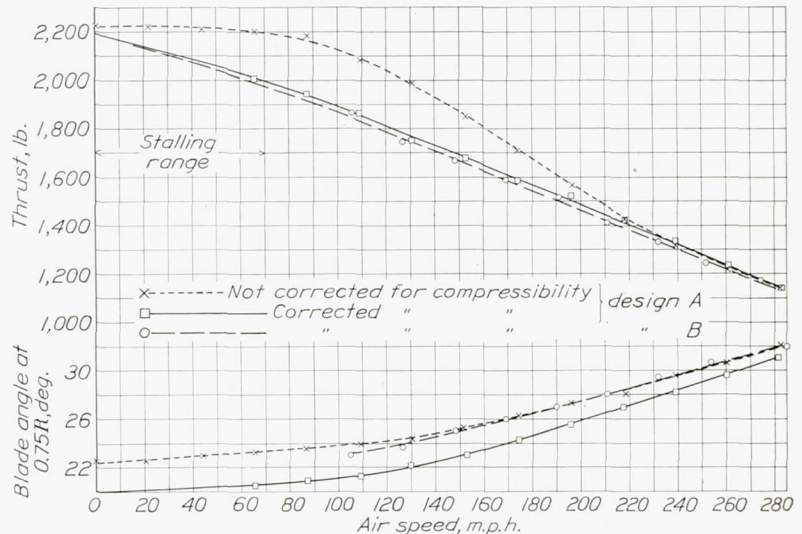
FIGURE 63.—Example 2 showing the uncorrected and corrected thrust and blade angles for an airplane equipped with propeller 5868–9 (controllable).
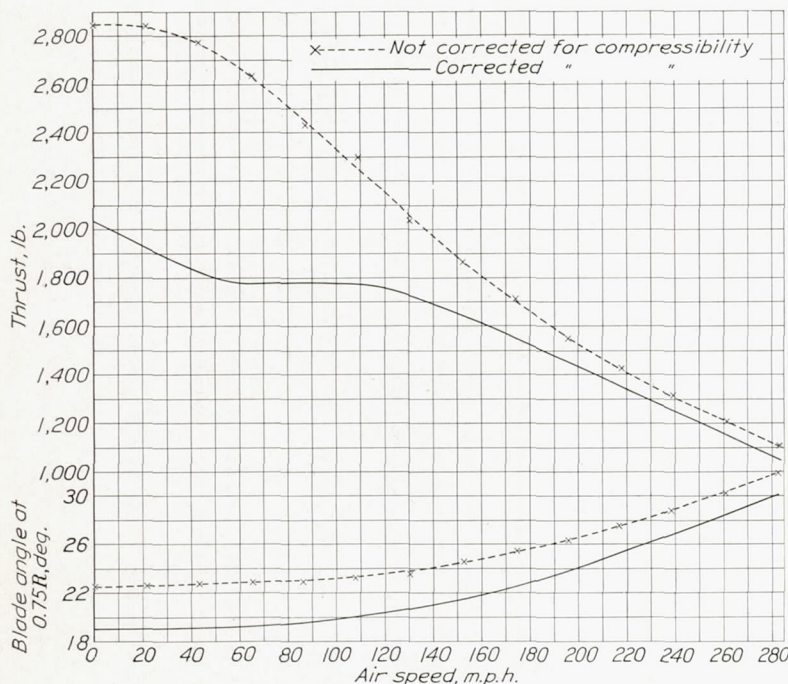
FIGURE 64.—Example 3 showing the uncorrected and corrected thrust and blade angles for an airplane equipped with propeller 5868–R6 (controllable).
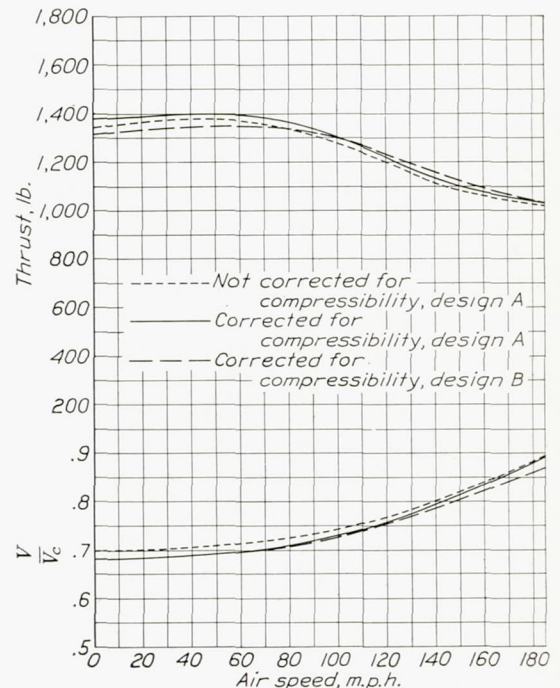
FIGURE 65.—Example 4 showing the uncorrected and corrected thrust and tip-speed ratios for an airplane equipped with propeller 5868–9 (fixed pitch).

uncorrected values obtained directly from the low-tip-speed data. It may be noted that the thrust curve is extrapolated to zero air speed, assuming that the effect of compressibility decreases as the angle of attack of the blade elements increases beyond the normal stall.

data; consequently, the design itself is slightly in error. In the use of the C_s chart mentioned, it is assumed that the propeller will absorb the power under certain specified conditions. Actually, the propeller will absorb more power at the tip speed of operation, so the blade

angle is reduced to make up for the difference. This result means that design A is a "compromise" design, because the diameter is slightly larger than it would be if there were no compressibility effects. If it were desired to eliminate the compromise feature, the design engine power could be reduced to correspond to the low-tip-speed data and the propeller could be selected on that basis. The following computations indicate the general procedure.

Selection of propeller—Design B:

$$\frac{C_P}{C_P \left(\frac{V}{V_c}=0.5\right)}=1.13 \text{ for high speed}$$

$$\text{hp.}_{(design)}=\frac{1,000}{1.13}=885$$

$$C_s=2.08$$

$$\frac{V}{nD}=1.34$$

$$D=7.83 \text{ feet}$$

$$\text{Tip speed}=972 \text{ f. p. s.}$$

$$V/V_c=0.867$$

$$C_{P(design)}=\frac{550\times1,000}{\rho\times\left(\frac{2,375}{60}\right)^3\times(7.83)^5}=0.1263$$

The computation of thrust and correction for compressibility effects are carried through in the same manner as for design A. No table is given but the results are plotted in figure 63. The thrust for design B is slightly less than for design A owing to the smaller diameter, even though the compressibility correction is less. No loss in high-speed thrust is evident for the compromise design A. It appears from this example that it is scarcely worth while to select propellers on the basis of corrected power unless the propeller diameter is too large on account of other considerations.

In example 3, a 3-blade 5868–R6 propeller is selected for the same requirements as given in example 2. In order to maintain the same tip speed as for design A, the same diameter propeller was assumed, although this size may not be the most efficient for high speed. Thrust computations are given in table I (c); the material is taken from figure 9 of reference 11 and figure 59 of this report. It happens that the test-body conditions were different for the 5868–9 and the 5868–R6 propellers but the body effects are small as compared with the compressibility effects. The results of the computations are given in figure 64. The loss in thrust due to com-

pressibility for this example is quite startling, amounting to about one-third of the uncorrected thrust at low tip speeds. Examples 2 and 3 illustrate the importance of compressibility when comparing propellers of different section. The R. A. F. 6 section is superior to the Clark Y section at low tip speeds but at high tip speeds the relative merits are reversed.

Fixed-pitch propellers.—The method of correcting fixed-pitch propellers is slightly more involved than for controllable propellers because the tip-speed correction changes with rotational speed. Unfortunately, each depends upon the other so, in order to obtain fairly exact results, a series of approximations is necessary. In the following examples the number of approximations has been minimized as far as is consistent with the importance of the corrections involved.

Example 4 illustrates the method of correcting fixed-pitch propellers used with unsupercharged engines.

Given:
Engine_ 600 horsepower.
Engine speed_ _ _ _ _ _ _ _ _ _ _ _ _ _ _ 2,375 r. p. m., sea-level operation.
Air speed_ _ _ _ _ _ _ _ _ _ _ _ _ _ _ _ _ 185 m. p. h.

Selection or design of propeller 5868–9 having three blades to be used with a radial engine nacelle:

Design A:

$$C_s=1.47$$

From figure 13 (reference 10),

$$\frac{V}{nD}=0.85$$

$$\beta=22.3°$$

Then

$$D=8.07 \text{ ft.}$$

$C_{P_1}=0.0653$ (design value for high speed).

Tip speed$=1,000$ f. p. s.

$$\frac{V}{V_c}=0.895.$$

$C_{T_1}=0.065$ (design value for high speed).

$$C_{T(at\ stall)}=0.140.$$

$$\frac{C_{T_1}}{C_{T(at\ stall)}}=0.465.$$

$$\frac{C_P}{C_P \left(\frac{V}{V_c}=0.5\right)}=1.115 \text{ (from fig. 58).}$$

This propeller will absorb 1.115×600 hp. or 670 hp. at high speed. Either the diameter or the blade angle must be reduced to absorb the specified 600 hp. Following the method of reducing the diameter, a new design is made using $\frac{600}{1.115}=538$ hp. This computation re-

sults in the following characteristics:

$$C_s = 1.503$$

$$\frac{V}{nD} = 0.9$$

$$D = 7.62 \text{ ft.}$$

$$\frac{V}{V_c} = 0.847$$

$$\frac{C_P}{C_{P\left(\frac{V}{V_c}=0.5\right)}} = 1.085$$

In view of the change in the power correction factor incurred by the reduced diameter and tip speed, this propeller will only absorb $538 \times 1.085 = 585$ hp. A third approximation using the average of the first and second values of $\frac{C_P}{C_{P\left(\frac{V}{V_c}=0.5\right)}}$ should result in approximately the correct answer; $\frac{1.115 + 1.085}{2} = 1.100$. The third approximation results in the following characteristics designated "design B":

$$\text{hp.} = \frac{600}{1.1} = 545 \text{ (for design purpose).}$$

$$C_s = 1.497$$

$$\frac{V}{nD} = 0.87$$

$$\beta = 22.7°$$

$$D = 7.88 \text{ ft.}$$

$$\text{Tip speed} = 978 \text{ f. p. s.}$$

$$\frac{V}{V_c} = 0.873$$

$$\frac{C_P}{C_{P\left(\frac{V}{V_c}=0.5\right)}} = 1.1 \text{ (check).}$$

In table II the thrust is computed for design B according to the following procedure:

1. In column 1, values of V/nD are assumed and, in addition, the design value for high speed is included.

2. From figure 10 (reference 10), the low-tip-speed power coefficients C_{P_2} are read following the line for a blade angle of 22.7°.

3. The corresponding thrust coefficient, C_{T_2}, is also read from figure 10 of reference 10.

4. The ratio N/N_{max} is computed from the relation $\frac{N}{N_{max}} = \sqrt{\frac{C_{P_2(at \; high \; speed)}}{C_{P_2}}}$, assuming that the torque

remains constant for small changes in rotational speed. This condition is substantially true for unsupercharged engines.

5. The ratio V/V_c is equal to $\frac{N}{N_{max}} \times 0.873$.

6. The ratio $\frac{C_{T_2}}{C_{T(at \; stall)}}$ is computed using $C_{T(at \; stall)} = 0.140$.

7. $\frac{C_P}{C_{P\left(\frac{V}{V_c}=0.5\right)}}$ is read from figure 58 for different values of V/V_c and $\frac{C_{T_2}}{C_{T(at \; stall)}}$.

8. $\frac{C_T}{C_{T\left(\frac{V}{V_c}=0.5\right)}}$ is also read from figure 58.

9. Corrected values of power coefficient C_{P_3} are computed, $C_{P_2} \times \frac{C_P}{C_{P\left(\frac{V}{V_c}=0.5\right)}} = C_{P_3}$.

10. Corrected values of thrust coefficient C_{T_3} are computed in a similar manner.

11. Corrected values of N/N_{max} are computed using C_{P_3}.

12. Values of V/V_{max} are computed from the relation $\frac{V}{V_{max}} = \frac{\left(\frac{V}{nD}\right)N}{\left(\frac{V}{nD}\right)_{max} N_{max}}$.

13. The air speed is computed from the relation V/V_{max}, knowing V_{max}.

14. The thrust is computed from the relation $T = C_T \frac{C_{P_3(at \; high \; speed)}}{C_{P_3}} \times K$, where $K = \rho n^2 D^4$.

If the method of reducing the blade angle is followed, to offset the increase in power coefficients from low to high tip speed, design A is used directly but it is necessary to determine the blade-angle reduction. The value of C_{P_1} is divided by $\frac{C_P}{C_{P\left(\frac{V}{V_c}=0.5\right)}}$ to determine the C_{P_2} corresponding to the low-tip-speed data; $\frac{0.0653}{1.115} = 0.0585$. Unfortunately, this value is only the first approximation because the low-tip-speed thrust coefficient is likewise reduced, changing the value of $\frac{C_{T_1}}{C_{T(at \; stall)}}$ to $\frac{0.059}{0.14}$ or 0.42. The value of $\frac{C_P}{C_{P\left(\frac{V}{V_c}=0.5\right)}}$ then becomes 1.105. The second approximate value of power coefficient becomes $\frac{0.653}{1.105} = 0.0592$. This C_{P_2} defines the blade angle so the C_{P_2} and C_{T_2} can be read from figure 10 (reference 10) for different values of V/nD. The corrected thrust is then computed in the manner outlined in table II. No table is included for design A

computations but the thrust is given in figure 65 together with those for design B and the uncorrected thrust.

It may be noted from figure 65 that little, if any, loss in thrust due to compressibility is evident for this example. The explanation lies in the fact that the tip speed drops to about 0.7 the speed of sound in the take-off range owing to the decrease in engine speed. It may be noted from figure 58 that a maximum of only 4 percent in efficiency is lost for this tip speed. It appears from this example that computations for correcting the thrust of fixed-pitch propellers may not be worth while in many instances. A preliminary estimate of the tip speed in the take-off range together with a reference to the correction factors would indicate the importance of further computations. It probably is desirable in any case to make allowances in the design of propellers for differences in the power coefficient for test data from low and high tip speeds in order to determine the diameter and the blade angle.

REFERENCES

1. Briggs, L. J., Hull, G. F., and Dryden, H. L.: Aerodynamic Characteristics of Airfoils at High Speeds. T. R. No. 207, N. A. C. A., 1925.
2. Stack, John: The N. A. C. A. High-Speed Wind Tunnel and Tests of Six Propeller Sections. T. R. No. 463, N. A. C. A., 1933.
3. Briggs, L. J., and Dryden, H. L.: Aerodynamic Characteristics of Twenty-Four Airfoils at High Speeds. T. R. No. 319, N. A. C. A., 1929.
4. Stack, John: The Compressibility Burble. T. N. No. 543, N. A. C. A., 1935.
5. Douglas, G. P., and Perring, W. G. A.: Wind-Tunnel Tests with High Tip Speed Airscrews.
    (a) The Characteristics of the Aerofoil Section R. A. F. 31a at High Tip Speeds. R. & M. No. 1086, British A. R. C., 1927.
    (b) The Characteristics of a Bi-Convex Aerofoil at High Speeds. R. & M. No. 1091, British A. R. C., 1927.
    (c) The Characteristics of Bi-Convex No. 2 Aerofoil Section at High Speeds. R. & M. No. 1123, British A. R. C., 1928.
    (d) The Characteristics of a Conventional Airscrew Section, Aerofoil R. & M. No. 322, No. 3, at High Speeds. R. & M. No. 1124, British A. R. C., 1928.
    (e) Some Experiments upon an Airscrew of Conventional Blade Section, Aerofoil R. & M. No. 322, No. 3, at High Speeds. R. & M. No. 1174, British A. R. C., 1928.
    (f) The Characteristics of a Conventional Airscrew Section 0.082c Thick and of R. A. F. 27 and R. A. F. 28. R. & M. No. 1198, British A. R. C., 1929.
6. Hartshorn, A. S., and Douglas, G. P.: Wind Tunnel Tests on High Tip Speed Airscrews. Further Experiments on Scale Effect. R. & M. No. 1417, British A. R. C., 1932.
7. Jennings, W. G., and Ormerod, A.: Full Scale Experiments on High Tip Speed Airscrews. The Effect of Thickness of Section on Airscrew Performance. R. & M. No. 1339, British, A. R. C., 1931.
8. Wood, Donald H.: Full-Scale Tests of Metal Propellers at High Tip Speeds. T. R. No. 375, N. A. C. A., 1931.
9. Weick, Fred E., and Wood, Donald H.: The Twenty-Foot Propeller Research Tunnel of the National Advisory Committee for Aeronautics. T. R. No. 300, N. A. C. A., 1928.
10. Biermann, David, and Hartman, Edwin P.: Tests of Five Full-Scale Propellers in the Presence of a Radial and a Liquid-Cooled Engine Nacelle Including Tests of Two Spinners. T. R. No. 642, N. A. C. A., 1938.
11. Biermann, David, and Hartman, Edwin P.: The Aerodynamic Characteristics of Six Full-Scale Propellers Having Different Airfoil Sections. T. R. No. 650, N. A. C. A., 1939.

TABLE I (a)

EXAMPLE 1, CONTROLLABLE PROPELLER

1	2	3	4	5	6	7	8	9	10	11	12	13
$\frac{V}{nD}$	β_1 for $C_{P_1}=0.0542$ (deg.)	C_{T_1} for β_1	$\dfrac{C_{T_1}}{C_T}$ (at stall)	$\dfrac{C_P}{C_P\left(\frac{V}{V_e}=0.5\right)}=\dfrac{C_{P_1}}{C_{P_2}}$	C_{P_2}	β_2 for C_{P_2} (deg.)	C_{T_2} for β_2	$\dfrac{C_T}{C_T\left(\frac{V}{V_e}=0.5\right)}=\dfrac{C_{T_3}}{C_{T_2}}$	C_{T_3}	Thrust (lb.)	Air speed (m.p.h.)	Remarks
0	19.9	0.0870	1.01	1.165	0.0465	18.5	0.0860	0.995	0.0855	2,100	0	Blades stalled.
.1	20.2	.0860	1.00	1.165	.0465	18.9	.0850	.995	.0845	2,075	19.3	
.2	20.7	.0860	1.00	1.165	.0465	19.0	.0845	.995	.0840	2,060	38.8	
.3	20.7	.0855	1.00	1.165	.0465	19.0	.0820	.995	.0815	2,000	58.2	Blades not stalled.
.4	20.6	.0822	.96	1.160	.0467	18.7	.0760	1.000	.0760	1,870	77.5	
.5	20.6	.0755	.88	1.150	.0471	19.0	.0695	1.010	.0703	1,727	97.0	
.6	20.9	.0680	.79	1.120	.0483	19.6	.0625	1.025	.0642	1,575	116.5	
.7	21.6	.0620	.73	1.120	.0483	20.3	.0555	1.060	.0589	1,445	135.5	
.8	22.3	.0550	.64	1.130	.0479	21.2	.0490	1.120	.0550	1,350	155.5	
.9	23.3	.0480	.56	1.130	.0479	22.3	.0435	1.130	.0493	1,215	175.0	
1.0	24.6	.0450	.53	1.130	.0479	23.7	.0395	1.130	.0446	1.095	194.0	

TABLE I (b)

EXAMPLE 2, CONTROLLABLE PROPELLER, DESIGN A

1	2	3	4	5	6	7	8	9	10	11	12	13
$\frac{V}{nD}$	β_1 for $C_{P_1}=0.1097$ (deg.)	C_{T_1} for β_1	$\dfrac{C_{T_1}}{C_T}$ (at stall)	$\dfrac{C_P}{C_P\left(\frac{V}{V_e}=0.5\right)}=\dfrac{C_{P_1}}{C_{P_2}}$	C_{P_2}	β_2 for C_{P_2} (deg.)	C_{T_2} for β_2	$\dfrac{C_T}{C_T\left(\frac{V}{V_e}=0.5\right)}=\dfrac{C_{T_3}}{C_{T_2}}$	C_{T_3}	Thrust (lb.)	Air speed (m.p.h.)	Remarks
0	22.5	0.1420	----	----	----	----	----	----	----	----	0	Blades stalled.
.1	22.5	.1417	----	----	----	----	----	----	----	----	21.8	
.2	23.0	.1410	----	----	----	----	----	----	----	----	43.6	
.3	23.3	.1405	1.00	1.240	0.0884	20.5	0.1320	0.970	0.1280	2,003	65.3	
.4	23.5	.1395	1.00	1.240	.0884	20.8	.1280	.970	.1240	1,945	87.1	Blades not stalled.
.5	24.0	.1330	.95	1.230	.0892	21.3	.1190	1.000	.1190	1,865	108.8	
.6	24.5	.1270	.91	1.220	.0900	22.2	.1095	1.020	.1115	1,750	130.5	
.7	25.3	.1180	.84	1.200	.0914	23.0	.1010	1.060	.1070	1,678	152.5	
.8	26.1	.1090	.78	1.185	.0925	24.3	.0930	1.090	.1012	1,588	174.0	
.9	27.3	.1000	.71	1.170	.0937	25.5	.0870	1.115	.0972	1,522	196.0	
1.0	28.0	.0910	.65	1.157	.0948	27.0	.0800	1.135	.0909	1,425	218.0	
1.1	29.5	.0840	.60	1.145	.0958	28.2	.0740	1.150	.0852	1,335	239.0	
1.2	30.5	.0780	.56	1.138	.0965	29.6	.0690	1.140	.0786	1,231	261.0	
1.3	32.0	.0730	.53	1.130	.0970	31.0	.0640	1.135	.0727	1,140	283.0	

TABLE I (c)

EXAMPLE 3, CONTROLLABLE PROPELLER

1	2	3	4	5	6	7	8	9	10	11	12	13
$\frac{V}{nD}$	β_1 for $C_{P_1}=0.1097$ (deg.)	C_{T_1} for β_1	$\dfrac{C_{T_1}}{C_T}$ (at stall)	$\dfrac{C_P}{C_P\left(\frac{V}{V_e}=0.5\right)}=\dfrac{C_{P_1}}{C_{P_2}}$	C_{P_2}	β_2 for C_{P_2} (deg.)	C_{T_2} for β_2	$\dfrac{C_T}{C_T\left(\frac{V}{V_e}=0.5\right)}=\dfrac{C_{T_3}}{C_{T_2}}$	C_{T_3}	Thrust (lb.)	Air speed (m.p.h.)	Remarks
0	22.6	0.1820	1.00	1.305	0.084	19.0	0.1730	0.75	0.1298	2,035	0	Blades stalled.
.1	22.6	.1810	1.00	1.305	.084	19.1	.1640	.75	.1230	1,928	21.8	
.2	22.8	.1770	.98	1.305	.084	19.2	.1530	.76	.1160	1,818	43.6	
.3	22.9	.1680	.94	1.305	.084	19.3	.1400	.79	.1105	1,730	65.3	
.4	23.0	.1550	.86	1.305	.084	19.5	.1290	.88	.1135	1,780	87.1	
.5	23.3	.1405	.79	1.305	.084	20.1	.1170	.97	.1133	1,780	108.8	
.6	23.6	.1300	.72	1.330	.0836	21.0	.1050	1.05	.1103	1,730	130.5	Blades not stalled.
.7	24.6	.1190	.66	1.355	.0810	21.5	.0900	1.13	.1029	1,610	152.5	
.8	25.4	.1090	.61	1.360	.0807	22.6	.0820	1.20	.0984	1,540	174.0	
.9	26.4	.0990	.55	1.350	.0813	24.1	.0760	1.22	.0932	1,460	196.0	
1.0	27.6	.0910	.51	1.330	.0825	25.2	.0700	1.23	.0862	1,350	218.0	
1.1	28.8	.0840	.47	1.310	.0838	27.0	.0640	1.23	.0791	1,240	239.0	
1.2	30.3	.0770	.43	1.290	.0850	28.3	.0590	1.23	.0729	1,145	261.0	
1.3	31.9	.0710	.40	1.275	.0861	30.0	.0550	1.24	.0682	1,070	283.0	

TABLE II

EXAMPLE 4, FIXED-PITCH PROPELLER, DESIGN B

1	2	3	4	5	6	7	8	9	10	11	12	13	14	15
$\dfrac{V}{nD}$	C_{P_2}	C_{T_2}	$\dfrac{N}{N_{max}}$ for C_{P_1}	$\dfrac{V}{V_c}$	$\dfrac{C_{T_2}}{C_{T\,(at\,stall)}}$	$\dfrac{C_P}{C_P\left(\frac{V}{V_c}=0.5\right)}$	$\dfrac{C_T}{C_T\left(\frac{V}{V_c}=0.5\right)}$	C_{P_3}	C_{T_3}	$\dfrac{N}{N_{max}}$ for C_{P_3}	$\dfrac{V}{V_{max}}$	Air speed (m.p.h.)	Thrust (lb.)	Remarks
0	0.1120	0.1420	0.780	0.680	1.01	1.050	1.020	0.1178	0.1448	0.796	0	0	1,314	Blades stalled.
.1	.1105	.1420	.780	.680	1.01	1.050	1.020	.1160	.1448	.802	.092	17.1	1,330	
.2	.1090	.1410	.790	.690	1.01	1.055	1.020	.1150	.1438	.806	.185	34.3	1,333	
.3	.1065	.1400	.800	.698	1.00	1.060	1.010	.1130	.1427	.813	.277	51.2	1,350	Blades not stalled.
.4	.1040	.1350	.809	.705	.96	1.060	1.025	.1100	.1385	.825	.379	70.1	1,343	
.5	.1000	.1280	.824	.719	.91	1.060	1.030	.1060	.1318	.839	.482	90.3	1,325	
.6	.0940	.1130	.850	.742	.81	1.052	1.040	.0990	.1175	.869	.599	111.0	1,270	
.7	.0860	.0970	.890	.777	.69	1.065	1.050	.0918	.1020	.902	.725	134.0	1,185	
.8	.0760	.0780	.945	.825	.56	1.085	1.080	.0825	.0842	.952	.875	162.0	1,090	
.87	.0680	.0660	1.000	.873	.48	1.100	1.100	.0747	.0726	1.000	1.000	185.0	1,038	
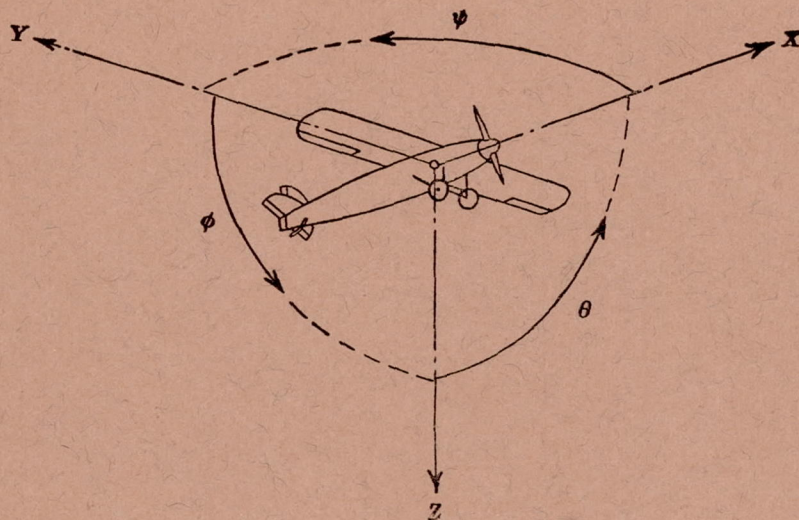
Positive directions of axes and angles (forces and moments) are shown by arrows

Axis		Force (parallel to axis) symbol	Moment about axis			Angle		Velocities	
Designation	Symbol		Designation	Symbol	Positive direction	Designation	Symbol	Linear (component along axis)	Angular
Longitudinal	X	X	Rolling	L	$Y \longrightarrow Z$	Roll	ϕ	u	p
Lateral	Y	Y	Pitching	M	$Z \longrightarrow X$	Pitch	θ	v	q
Normal	Z	Z	Yawing	N	$X \longrightarrow Y$	Yaw	ψ	w	r

Absolute coefficients of moment

$$C_l = \frac{L}{qbS} \qquad C_m = \frac{M}{qcS} \qquad C_n = \frac{N}{qbS}$$
$$\text{(rolling)} \qquad \text{(pitching)} \qquad \text{(yawing)}$$

Angle of set of control surface (relative to neutral position), δ. (Indicate surface by proper subscript.)

4. PROPELLER SYMBOLS

D,   Diameter

p,   Geometric pitch

p/D,   Pitch ratio

V',   Inflow velocity

V_s,   Slipstream velocity

T,   Thrust, absolute coefficient $C_T = \dfrac{T}{\rho n^2 D^4}$

Q,   Torque, absolute coefficient $C_Q = \dfrac{Q}{\rho n^2 D^5}$

P,   Power, absolute coefficient $C_P = \dfrac{P}{\rho n^3 D^5}$

C_s,   Speed-power coefficient $= \sqrt[5]{\dfrac{\rho V^5}{Pn^2}}$

η,   Efficiency

n,   Revolutions per second, r.p.s.

Φ,   Effective helix angle $= \tan^{-1}\left(\dfrac{V}{2\pi rn}\right)$

5. NUMERICAL RELATIONS

1 hp.=76.04 kg-m/s=550 ft-lb./sec.

1 metric horsepower=1.0132 hp.

1 m.p.h.=0.4470 m.p.s.

1 m.p.s.=2.2369 m.p.h.

1 lb.=0.4536 kg.

1 kg=2.2046 lb.

1 mi.=1,609.35 m=5,280 ft.

1 m=3.2808 ft.